A special envelope separates extra-chromosomal from chromosomal DNA in the cytoplasm of mammalian cells

Laura Schenkel, Xuan Wang, Nhung Le[+], Michael Burger and Ruth Kroschewski
ETH Zürich, Institute of Biochemistry, Otto-Stern-Weg 3, 8093 Zürich, Switzerland

[+] current address:
VNU University of Science, 334 Nguyen Trai street, Thanh Xuan district, Hanoi city, Vietnam.

Abstract

In eukaryotes, chromosomes are wrapped in an endoplasmic reticulum (ER)-derived envelope to form the nucleus. Whether any DNA, or only chromosomes, can be enveloped in this way is unclear. Live-cell imaging revealed that DNA transfected into mammalian cells was either captured directly in the cytoplasm, or if it entered the nucleus was soon expelled from it. In the cytoplasm, plasmid DNA was rapidly surrounded by an ER-derived double membrane and frequently colocalized with extra-chromosomal DNA of telomeric origin expelled from the nucleus. Therefore, this structure was termed exclusome. Exclusome membranes contain the inner-nuclear membrane proteins Lap2β and Emerin but differ from the nuclear envelope by the absence of the Lamin B Receptor, nuclear pore complexes (NPCs) and by the presence of fenestrations. Strikingly, Emerin was strongly enriched at exclusomes and overexpression of its LAP2, Emerin, MAN1 (LEM)-domain reduced cells with exclusomes. Together, cells wrap chromosomes and two types of extra-chromosomal DNA into similar yet distinct envelopes. Thereby, they distinguish, sort, cluster, package, and keep chromosomal and extra-chromosomal DNA apart in the nucleus and the exclusome, respectively. We suggest that while all DNA molecules are enveloped through virtually identical mechanisms, only chromosomes somehow promote NPC assembly to form a nuclear envelope.

Introduction

In all eukaryotes the genome is enclosed in the nucleus, which compartmentalizes the chromosomes away from the cytoplasm (Güttinger et al., 2009). The separation between nucleoplasm and cytoplasm is ensured by a flat double membrane derived from the endoplasmic reticulum (ER). Exchange between the nucleoplasm and the cytoplasm occurs mainly through pores in this double membrane which are made selective by nuclear pore complexes (NPCs). Such NPC-containing double membrane is further specialized, e.g., by the presence of inner-nuclear membrane (INM) proteins, constituting the nuclear envelope. In many species, the nuclear envelope breaks down in mitosis and reassembles around the chromosomes upon mitotic exit. Whether nuclear envelope assembly is somehow restricted to chromosomes at the end of mitosis or if it can take place around any DNA in the cytoplasm and even throughout the cell cycle is unknown.

How mammalian cells assemble the nuclear envelope at the end of mitosis has been intensively studied. When the separated chromosomes are pulled to opposite spindle poles towards the end of anaphase, tubular ER membranes approach each segregating chromosomal mass from several sides establishing the beginnings of two nuclear envelopes (Anderson & Hetzer, 2008). In parallel, Barrier-to-autointegration factor (BAF, BANF), which sequence unspecifically binds DNA, accumulates at the surface of mitotic chromosomes (Samwer et al., 2017; Zheng et al., 2000). BAF is required for wrapping the chromosomes in membranes, which contain several transmembrane proteins of the LAP2, Emerin, MAN1 (LEM)-domain family (Haraguchi et al., 2001; Kobayashi et al., 2015). BAF binds to the LEM-domain of e.g., Emerin, and thereby establishes a DNA membrane tether (Lee et al., 2001). NPC assembly occurs subsequently at areas of the separating chromosomal masses where spindle microtubules are not present. Specifically, NPCs are inserted as pre-pores into the membrane sheets that already associated with chromosomes (Otsuka et al., 2018). Would these events indistinctively take place and wrap up any type of DNA or are they exclusive to chromosomes?

In addition to the special case of mitochondria, there are situations *in vivo* where DNA is enwrapped by a membrane. For example, late in anaphase, lagging chromosomes can be enwrapped in an envelope and thus separate from the main nucleus, forming structures called micronuclei. Initially, the micronuclear envelope has all the characteristics of a nuclear envelope (Hatch et al., 2013). However, it degenerates over time. Over this period the enclosed DNA becomes fragmented and during one of the following mitoses the fragments reintegrate into chromosomes (Crasta et al., 2012; Zhang et al., 2015). In micronuclei, loss of

Lamin B1 correlates with their decay (Hatch et al., 2013). It is not known, however, what makes micronuclei degenerate while the nucleus stays intact. Remarkably, lagging chromosomes were shown to be frequent. Yet, they were transient, hardly forming micronuclei, as they mostly reintegrated during the mitosis in which they appeared into the reforming nucleus in human non-transformed and transformed cell lines (Orr et al., 2021). Also in *Drosophila melanogaster* neuronal stem cells, chromatin fragments originating from chromosome ends were rarely found in micronuclei (Karg et al., 2015). Instead, these fragments either rejoined early in anaphase a membrane-free chromosomal mass or they rejoined newly formed nuclei via nuclear envelope channels and by tethering to chromosome ends later in anaphase (Karg et al., 2015; Warecki et al., 2020). Thus, lagging chromosomes mostly rejoin nuclei within the same mitosis or they form less frequently unstable micronuclei, where the fragmented micronuclear DNA ends up in nuclear chromosomes after some divisions. Remarkably, syncytia, which are cells with multiple stable nuclei, exist. All these nuclei are roughly of similar size as seen in the slime mold *Physarum polycephalum* and human osteoclasts (Gerber et al., 2022; Kopesky et al., 2014). In contrast micronuclei in mammalian cells are at least 5 times smaller than their corresponding nuclei (Kneissig et al., 2019). Therefore, separate nuclei and nucleus-like structures can form in the same cell but in many instances the smaller structures are unstable.

Remarkably, circular extra-chromosomal DNA excised from chromosomes, thus of endogenous origin, exists in every cell type tested (Noer et al., 2022; Paulsen et al., 2018). However, extra-chromosomal DNA can also be of exogenous origin. Remarkably, when lambda phage or plasmid DNA was mixed with *Xenopus* oocyte extracts, it was subsequently enwrapped by a nuclear envelope, which could suggest that any DNA can be enveloped by a nuclear envelope (Blow & Laskey, 1986; Newport, 1987). Thus, exogenous extra-chromosomal DNA introduction into cells by e.g., viral or bacterial infections or transfection provide opportunities to study the formation of nucleus-like structures, as well as help to understand how cells distinguish chromosomal from extra-chromosomal DNA. Therefore, in this study we have introduced DNA into the cytoplasm of mammalian somatic cells and characterized its enwrapping by membranes. Particularly, we investigated the similarities and differences between such membranes and a bona fide nuclear envelope.

Results

Cells sort transfected plasmid DNA to the cytoplasm

We chose to study the association of plasmid DNA with membranes after its transfection into human tissue culture cells, as its visualization is established. To visualize transfected plasmid DNA, we used the LacO/LacI-system, where a plasmid containing 256 repeats of the Lactose (Lac) Operon (pLacO) is introduced into cells stably expressing Lac Inhibitor (LacI) fusion protein with either GFP or mCherry as fluorescence tag. Here, we employed three different HeLa cell lines (hereafter referred to as “HeLa-LacI”) and transfected them with pLacO to analyze the localization of transfected plasmid DNA. Fluorescent LacI foci in the cytoplasm were detected in cells transfected with plasmid DNA either by lipofection or electroporation (two methods to introduce plasmid) (SFig. 1; as previously reported in (Wang et al., 2016)). Due to the presence of a nuclear localization sequence (NLS) in the LacI fusion protein, the nuclear LacI fluorescence generally masked signals coming from plasmids in the nucleus. These results confirm that the LacI foci report plasmid localization in cells after transfection; hereafter, we refer to these LacI foci as plasmid foci. We first used this reporter system to study the localization and dynamics of plasmid foci. To do so we performed time-lapse live-cell microscopy for up to 24 hours (Fig. 1A-D, SFig. 2, SFig. 3). We started image acquisition concomitantly with the addition of the plasmid-lipofection mix to the cells and under conditions that preserved viability in the dividing cell population (SFig. 2A).

We observed the formation of plasmid foci throughout the imaging period, perhaps because plasmids continuously entered the cells (Fig. 1B, SFig. 2B). Most of these plasmid foci (89 %) persisted throughout the entire imaging period (Fig. 1B). The other plasmid foci (11 %) were visible for variable durations (between 30 min and 17 hours) before disappearing (Fig. 1B, SFig. 2C). Consistent with our previous study, most cells exhibited only one plasmid focus (63 %; SFig. 2D, (Wang et al., 2016)). Next, we analyzed the history of cells with a single focus at the end of imaging (211 cells, 63 % of all cells with ≥ 1 plasmid foci, 19% of all imaged cells at the end of imaging). Interestingly, we found that 76 % of cells with one plasmid focus had either formed only a single plasmid focus or inherited it during mitosis. In contrast, partitioning of multiple foci during mitosis or disappearance of foci (21 % and 3 %, respectively) contributed less to the cells with one plasmid focus at the end of imaging. Notably, we did not observe any plasmid foci fusion events under our imaging conditions (SFig. 2E,F; total 291 plasmid foci in 114 cells over up to 24 hours). These data show that transfected cells usually form only one plasmid focus. Once formed, plasmid foci are generally stable.

Our live-cell imaging also revealed that 58 % of plasmid foci formed during interphase, while the other 42 % were plasmid foci formed during mitosis, away from the chromosomal mass (Fig. 1A, mitotic formation, bold time point,C, SFig. 2I). Amongst the plasmid foci formed during interphase 88 % formed in the cytoplasm and 12 % in the nucleus (Fig. 1A,C, SFig. 2G). Next, we analyzed the location of each appearing plasmid focus at the end of imaging. Irrespective of where and when plasmid foci formed, all but one ended up in the cytoplasm (Fig. 1A at 24 h,D, SFig. 2H,I).

Next, we wondered how plasmid foci formed in the nucleus entered the cytoplasm. Focusing on plasmid foci formed in the inner nucleoplasm, we observed two different translocation modes: 13 out of 15 such plasmid foci entered the cytoplasm during mitosis by being sorted away from the chromosomal mass (SFig. 3A (1st example),B). The other two plasmid foci left the nucleus during interphase by nuclear budding (SFig. 3A (2nd example),B), revealing that the cell employs at least two ways to exclude plasmid DNA from the nucleus.

These data make four points. First, most of the plasmid DNA becomes LacI-associated in the cytoplasm and remains there, possibly without ever reaching the nucleus. Second, there are two modes for nuclear plasmid to partition away from the chromosomes: through expulsion via nuclear budding from the interphase nucleus (SFig. 3A (2nd example)) or through separation from the chromosomal mass during mitosis (mitotic sorting, Fig. 1A upper panel 9.5 hours, and bottom panel 4.5 hours, SFig. 2I, SFig. 3A (1st example),B). Third, the sorting of plasmid DNA from chromosomal DNA occurs rapidly; plasmid foci formed either during mitosis or in the nucleus during interphase relocated to the cytoplasm within 1 hour after their appearance (median, SFig. 3C). Fourth, in contrast to micronuclei formed by lagging chromosomes or parts of them, plasmid foci formed during mitosis are predominantly formed before (88 % of mitotically appearing plasmid foci) and not during anaphase, when chromosomal fragments or lagging chromosomes become visible as distinct units (SFig. 3D,E). Furthermore, plasmid foci unlike micronuclei never formed in the region between the separating chromosomes during anaphase (Fig. 1A, mitotic formation 4.5 hours, SFig. 3D,E, (Liu et al., 2018; Orr et al., 2021; Wang et al., 2016)). Therefore, we conclude that the dynamics of LacI decorated plasmid DNA are distinct from the mitotic separation of chromosomal fragments or lagging chromosomes from the chromosomal mass. Finally, most plasmid foci are formed during interphase (58 %) and are thus not mitotic products in contrast to micronuclei. Overall, these data reveal that HeLa cells have three ways to specifically sort plasmid DNA away from the chromosomes and that the cell collects plasmid DNA in the cytoplasm where it persists.

177 **Cytoplasmic plasmid foci remain separated from chromosomes over extended periods**
178 **of time**
179 Next, we extended the period of live cell imaging up to 122.5 hours to assess if the separation
180 between chromosomes and plasmid DNA is maintained for long time periods (Fig. 1E,F).
181 About 2/3 of the cytoplasmic plasmid foci were maintained and stayed separated from
182 chromosomes during this period, frequently being propagated over 3 cell divisions. The
183 fluorescence of about 1/3 of the foci however decayed over more than 10 hours, before
184 disappearing (Fig. 1F). Since the fluorescence decay occurred only at some plasmid foci within
185 a whole field of view, it was not due to bleaching, but suggests that the DNA was degraded
186 (SFig. 4). Cytoplasmic plasmid foci remained in the cytoplasm during the imaging period and
187 we never observed entry into the nucleus (Fig. 1E, SFig. 4), in contrast to what is reported for
188 DNA of micronuclei (Crasta et al., 2012; Zhang et al., 2015). Thus, even up to 122.5 hours
189 after transfection, plasmid foci behaved similarly to early periods after lipofection. Thus, the
190 separation between chromosomal DNA and plasmid DNA is persistent over several divisions,
191 consistent with (Wang et al., 2016).
192
193 **Cells harboring a single cytoplasmic plasmid focus are dominant under diverse**
194 **conditions**
195 We next studied whether these observations were time- and plasmid type-dependent and
196 occurred in other cell types. We have previously shown that most pLacO lipofected MDCK
197 cells (non-transformed canine kidney cells) predominantly had one cytoplasmic focus per cell,
198 24 hours after transfection. Here we assessed how MDCK-LacI and HeLa-LacI cells handled
199 plasmid DNA at different times after electroporation and lipofection (SFig. 5A-C). Two critical
200 results are highlighted here. First, in both cell lines and employing both transfection methods,
201 most cells with plasmid foci (grouped into classes of 1- and various multi-foci cells) had a
202 single plasmid focus, regardless of the time point after transfection (3 hours – 72 hours; SFig.
203 2D, SFig. 5C). Further, the analysis of the electroporation experiments shows that at 3 hours
204 the sum of all different classes of cells with multiple foci pooled together (61 %) is larger than
205 the fraction of cells with only one focus (39 %). This ratio changed over time. Notably, between
206 24 hours and 72 hours after transfection, the fraction of multi-foci cells decreased strongly,
207 while that of the 1-focus cells increased (1-focus cells: 50 % at 24 hours; 82 % at 72 hours).
208 As this occurred in the absence of further plasmid uptake - in contrast to lipofection - the data
209 suggests that either multi-foci cells died, or a single cytoplasmic focus is differentiated from
210 other plasmid foci in a cell and selectively maintained.
211
212

213 We next tested if the LacO repeat sequence had any effect on the cytoplasmic localization of
214 transfected plasmids. For this, we lipofected plasmids with and without LacO repeats and with
215 or without coding sequences into HeLa cells. Subsequently, we used FISH to visualize these
216 plasmids (SFig. 5D-F). For all tested plasmids, most focus-containing cells had a single
217 cytoplasmic focus 24 hours after lipofection, similar to our experiments where we visualized
218 pLacO with LacI fluorescence (SFig. 5E,F). These results show that plasmid DNA is
219 preferentially maintained in a single plasmid focus in the cytoplasm of mammalian cells,
220 regardless of the cell line, plasmid type, or transfection method.
221
222 **Plasmid DNA localizes to the cytoplasm in an ER-enwrapped compartment**
223 The cytoplasmic plasmid foci are ideal to assess if and which membrane is associated with
224 them. As the nuclear envelope originates from the endoplasmic reticulum (ER) and ER is
225 abundant in the cytoplasm, we first quantitatively characterized the association of plasmid
226 DNA with ER. 24 hours after pLacO lipofection into HeLa-LacI cells expressing either the ER
227 transmembrane reporter Sec61-mCherry (Fig. 2A) or the ER-lumen reporter eGFP-KDEL (Fig.
228 2B), all cytoplasmic plasmid foci colocalized with both ER reporters. Immunofluorescent
229 detection of the ER-residing LEM-domain protein LEM4 (ANKLE2) confirmed the presence of
230 ER at all cytoplasmic plasmid foci 24 hours after lipofection (Fig. 2C) or electroporation (SFig.
231 6A). The intensities of the ER-reporters KDEL and LEM4 were similar at the plasmid focus
232 compared to the overall ER in 71 % to 91 % of the cases, (category referred to as "non-
233 enriched", Fig. 2B,C, SFig. 6A). However, the intensity of the ER transmembrane marker
234 Sec61 was frequently higher at the plasmid focus compared to the overall ER (category
235 referred to as "enriched" in 61 % of the cases, Fig. 2A, SFig. 6A). Thus, ER membrane and
236 lumenal ER proteins were always present at the cytoplasmic plasmid focus, suggesting that a
237 double membrane encloses the plasmid DNA, reminiscent of the nuclear envelope.
238
239 **A special double membrane enwraps cytoplasmic plasmid DNA**
240 To visualize the cytoplasmic plasmid focus at higher resolution, we used correlative light and
241 electron microscopy (CLEM) in interphase HeLa cells 24 hours after pLacO lipofection. In
242 these images, a double membrane enclosing the cytoplasmic plasmid focus is clearly visible
243 (Fig. 3A, yellow arrowheads in the blue inset) similarly to the nuclear envelope (yellow
244 arrowheads in the green inset). The membrane surrounding the plasmid focus has
245 fenestrations, indicating that it may be an open compartment (green arrowheads in the blue
246 inset). Moreover, this membrane connects to the ER (red arrowhead in the blue inset),
247 consistent with the presence of ER proteins at plasmid foci. The cytoplasmic plasmid focus
248 has a higher electron density than the interphase chromosomes in the nucleus suggesting a
249 denser DNA packing in the plasmid focus. Overall, aside from the fenestrations, this

250 compartment's membrane organization is highly reminiscent of the nuclear envelope
251 surrounding chromosomal DNA.
252
253 To further investigate the similarities between the membrane enclosing the plasmid focus and
254 the nuclear envelope, we probed for the presence of inner nuclear membrane proteins at
255 cytoplasmic plasmid foci 24 hours after transfection with pLacO. We paid particular attention
256 to those that could participate in a DNA-membrane tethering at cytoplasmic plasmid foci. One
257 tether at the nuclear envelope is composed of BAF and INM-membrane proteins with a LEM-
258 domain, like Emerin or Lap2β (Ibrahim et al., 2011; Lee et al., 2001; Zheng et al., 2000).
259 Remarkably, cytoplasmic plasmid foci always contained BAF alongside Emerin and Lap2β
260 (Fig. 3B,C,E) (Ibrahim et al., 2011; Kobayashi et al., 2015). BAF was in addition always
261 enriched at plasmid foci compared to the nuclear envelope suggesting a high density of
262 plasmid molecules. More remarkable is that Emerin was enriched at nearly all foci (90 %, Fig.
263 3E, SFig. 6B). Lap2β was less frequently enriched (40 %; Fig. 3E, SFig. 6B). These results
264 suggest that LEM-domain proteins and BAF might tether plasmid DNA to surrounding ER
265 membranes. Another known tether at the nuclear envelope involves the transmembrane
266 protein Lamin B Receptor (LBR), which binds to heterochromatin protein 1, repressing
267 transcription in the nearby chromatin (Ye & Worman, 1996). LBR was not detected at plasmid
268 foci (Fig. 3D,E). Therefore, we conclude that this second DNA-membrane tether is missing.
269 Overall, the double membrane around the cytoplasmic plasmid focus has both similarities
270 (presence of Emerin and Lap2β) and differences (fenestrations, absence of LBR, enrichment
271 of Emerin) to the nuclear envelope.
272
273 **The special double membrane enwrapping cytoplasmic plasmids is devoid of**
274 **functional NPCs**
275 Next, we probed for NPCs in the membrane around cytoplasmic plasmid foci in HeLa cells,
276 24 hours after transfection with pLacO. NPCs appear to be absent, as both FG-repeat
277 containing Nuclear pore proteins (NUPs; anti-FG repeat) and Embryonic Large Molecule
278 Derived From Yolk Sac (ELYS), which is required for NPC assembly (Rasala et al., 2006),
279 were both absent from cytoplasmic plasmid foci in 94 % of the cases (Fig. 4A). The rare cases
280 when these proteins are present at the plasmid focus might reflect remnants of nuclear
281 budding events. The transmembrane protein Nuclear Envelope Pore Membrane 121
282 (POM121) was always absent at plasmid foci (Fig. 4B). We also probed for evidence of NPC-
283 mediated nuclear-cytoplasmic transport at cytoplasmic plasmid foci. Here, we observed that
284 the Importin β-binding Domain (IBB-GFP) was always absent (Fig. 4C). In addition, the
285 nucleotide exchange factor for Ran (Regulator of Chromatin Condensation 1, RCC1), which

286 supports NPC formation and establishes a Ran-gradient across the enclosing membrane, was
287 never detected at cytoplasmic plasmid foci (Fig. 4D, (Walther et al., 2003)). We conclude that
288 the double membrane enclosing cytoplasmic plasmid DNA is devoid of functional NPCs.
289
290 The EM analysis indicated that the cytoplasmic plasmid compartment is not entirely closed
291 (Fig. 3A). Therefore, we tested whether soluble GFP could access the cytoplasmic plasmid
292 compartment by Fluorescence Recovery After Photobleaching (FRAP) in HeLa-LacI cells 24
293 hours after lipofection of pLacO. The GFP fluorescence was bleached at the cytoplasmic
294 plasmid focus and a reference area in the cytoplasm (Fig.4 E-G). Fluorescence recovery took
295 place in both areas, with the recovery time (the time when half of the bleached signal is
296 recovered, $t_{1/2}$) being slightly longer for areas containing the plasmid focus (1.8 times),
297 showing that the diffusion of GFP molecules into the plasmid focus is hindered, but not
298 abolished. Thus, the special double membrane enclosing cytoplasmic plasmid DNA, while
299 devoid of functional NPCs, still allows exchange with the cytoplasm.
300
301 **A plasmid focus formed in the cytoplasm is rapidly enwrapped by membrane**
302 The nuclear membrane rapidly encloses chromosomal DNA at the end of mitosis. Therefore,
303 we assayed the time scale of membrane association with cytoplasmic plasmid DNA. We used
304 HeLa cells stably expressing Lap2β-GFP and transiently expressing LacI-mCherry without
305 NLS to ensure enough LacI was present in the cytoplasm, allowing early cytoplasmic plasmid
306 visualization. In addition, the cells were thymidine-synchronized to ensure a higher
307 homogeneity of the cell population. These cells were lipofected with pLacO and imaged every
308 15 min for 25.25 hours starting after the addition of the lipofection-DNA mix to analyze
309 appearing plasmid foci (Fig. 5). 51 % of such plasmid foci were already associated with
310 membrane at their appearance, as reported by Lap2β (Fig. 5D). Over time, plasmid foci were
311 increasingly associated with Lap2β-containing membrane. Finally, 75 min after appearance,
312 97 % of the plasmid foci were Lap2β-membrane-associated (Fig. 5D). Thus, membrane
313 association appears to accompany plasmid focus appearance (Fig. 5C,D).
314
315 **Emerin is enriched at cytoplasmic plasmid compartments in primary human cells**
316 To probe if the special double membrane can also form around cytoplasmic plasmid foci in
317 non-immortalized cells, we transfected primary human fibroblasts with pLacO and visualized
318 the plasmid with transiently expressed LacI-NLS-GFP. In addition, we immunostained the cells
319 for Emerin or LEM4 (Fig. 6A,B). We noticed that these primary cells divided significantly less
320 frequently than HeLa cells and therefore analyzed the cells 48 hours after pLacO transfection.
321 Also here, most transfected cells had a single plasmid focus (SFig. 6C). Emerin was present

322 at each plasmid focus amongst cells with one plasmid focus and even enriched in 97 % of the
323 instances compared to the surrounding ER or nuclear envelope (Fig. 6A). Also, all plasmid
324 foci in multi-foci cells were Emerin positive apart from one cell, where three foci didn't
325 colocalize with Emerin, possibly because the reaction to transfection is delayed in these
326 primary cells compared to HeLa cells (SFig. 6D). Remarkably, in multi-foci cells, several
327 plasmid foci of a single cell were Emerin enriched (SFig. 6D,F). Similarly, LEM4 was always
328 present in cells with one plasmid focus and, in 45 % of these cells, even enriched compared
329 to the surrounding ER. This is qualitatively similar to HeLa cells (Fig. 6B). In multi-foci cells
330 LEM4 was always present, except for 2 plasmid foci in two different cells (SFig. 6E).
331
332 Thus, both in primary human fibroblasts as well as in HeLa cells, plasmid DNA is excluded
333 from the nucleus and localizes to the cytoplasm where it exists predominantly in one
334 membranous organelle. We term this organelle the exclusome. A diagnostic hallmark of the
335 exclusome is that Emerin is enriched as compared to the nuclear envelope. The exclusome
336 envelope is further characterized by the presence of fenestrations, presence of Lap2β,
337 presence and even occasional concentration of ER-membrane proteins like Sec61 or LEM4,
338 and the absence of NPCs and LBR.
339
340 **Interference with Emerin's function reduces the compartmentalization of plasmid DNA**
341 **in the cytoplasm**
342 Since Emerin is enriched at ~90 % of plasmid foci and the formation of a double membrane is
343 concomitant with plasmid focus formation (Fig. 3B,E, Fig. 5), we speculated that Emerin might
344 tether plasmid DNA to the surrounding membrane to establish an exclusome. As Emerin's
345 LEM-domain binds BAF and BAF binds DNA (Lee et al., 2001), we aimed to interfere with this
346 molecular linkage. To do so, we chose to interfere with the function of Emerin's LEM-domain
347 by setting up a competition approach with an excess of the soluble LEM-domain of Emerin.
348 Specifically, we overexpressed either the LEM-domain of Emerin fused to GFP and a nuclear
349 export signal ("GFP-LEM") or soluble GFP ("GFP") (Fig. 7A, left side) as a control in
350 synchronized HeLa-LacI cells. Subsequently, pLacO was electroporated and cells that
351 expressed GFP-LEM or GFP were analyzed (Fig. 7A, right side). The competition was
352 successful for two reasons. First, Emerin was less enriched at the nuclear envelope and more
353 present in the ER in cells expressing GFP-LEM compared to control cells expressing GFP.
354 This suggests that the overexpression of GFP-LEM competed with endogenous Emerin for
355 DNA tethering at the nuclear envelope, thus leading to reduced Emerin retention at the nuclear
356 envelope and re-localization to the ER (SFig. 7B,C). Second, Emerin associated also less
357 frequently with cytoplasmic plasmid foci at two time points after pLacO transfection in cells
358 expressing GFP-LEM compared to the control (Fig. 7B, SFig. 7D).

359 The amino acid sequences of the LEM-domains of Emerin and LEM4 are 44 % similar (SFig.
360 7A). Because of this, the overexpressed LEM-domain of Emerin might also interfere with the
361 function of other LEM-domain proteins. To test for this possibility and to further characterize
362 the plasmid focus membrane, we probed for the presence of LEM4. The association of LEM4
363 was not affected in GFP-LEM expressing cells at either 6 hours or 24 hours after pLacO
364 electroporation (Fig. 7C, SFig. 7E). Moreover, LEM4 was present in all conditions at almost
365 all cytoplasmic plasmid foci (99 %, mean of 3 to 5 exp., all conditions), revealing that even
366 Emerin-negative plasmid foci are membrane-enclosed. Furthermore, the presence of LEM4
367 in Emerin-negative plasmid foci indicates that other proteins might compensate for Emerin's
368 function, although clearly less efficiently.
369
370 Since we could interfere with Emerin's function, we went on to characterize the effects of GFP-
371 LEM overexpression on the cell's reaction towards transfected plasmid DNA. We determined
372 how many cells expressing GFP-LEM or GFP, had at least one cytoplasmic plasmid focus. In
373 the GFP-LEM condition, fewer cells contained at least one cytoplasmic plasmid focus
374 compared to control, both 6 hours and 24 hours after pLacO transfection (36 % for GFP-LEM
375 and 66 % for GFP; Fig. 7D). At 24 hours after transfection, the number of cells with plasmid
376 foci were halved in both conditions compared to the 6-hour time point due to cell division and
377 asymmetric partitioning of the plasmid foci (16 % for GFP-LEM and 35 % for GFP). Together,
378 these data suggest that Emerin, through its LEM-domain, supports the compartmentalization
379 of plasmid DNA within the cytoplasm of mammalian cells.
380
381 **Exclusomes can contain telomeric DNA**
382 In cells undergoing alternative lengthening of telomeres (ALT), like the osteosarcoma cell line
383 U2OS, circular extra-chromosomal DNA of telomeric origin is abundant (Cesare & Griffith,
384 2004). Remarkably, in U2OS and several other cancer cell lines, such as WI38-VA13, SaOs2,
385 and KMST-6, between 1 and 4 FISH signals of extra-chromosomal telomeric DNA were
386 detected in the cytoplasm (Chen et al., 2017; Tokutake et al., 1998). In addition, several
387 groups have detected circular extra-chromosomal telomeric DNA in non-ALT cancer cells like
388 HeLa (Regev et al., 1999; Tokutake et al., 1998; Vidaček et al., 2010; Wang et al., 2004).
389 Therefore, we decided to test whether this extra-chromosomal DNA of endogenous origin is
390 membrane-enclosed in the cytoplasm and whether this membrane shares similarities with the
391 nuclear envelope or the exclusome.
392
393 We performed FISH experiments in U2OS and HeLa cells using two different fluorescently
394 tagged telomeric probes (TelC and TelG). In all cases, we observed numerous FISH signals
395 in the nuclei and few in the cytoplasm (Fig. 8A,B, SFig. 8A,B). We also demonstrated that the

396 cytoplasmic Tel FISH signals were not artifacts caused by clustered probes as cells
397 simultaneously hybridized with both a telomeric probe as well as a scrambled probe only
398 showed telomeric probes signals (SFig. 8A-C). Further, both types of cytoplasmic telomeric
399 FISH signals indeed labeled DNA, as a DNaseI treatment prior to probe hybridization
400 abolished the signal (SFig. 8D,E).
401
402 Micronuclei with chromosomal fragments frequently occur in cancer cells. To exclude such
403 compartments from our analysis, we chose Hoechst fluorescence as a criterium, as the
404 median size of circular ex-tDNA is only 5 kb (Cesare & Griffith, 2004). Based on this criterium,
405 we distinguished two types of tDNA in the cytoplasm of both HeLa and U2OS cells: tDNA in
406 Hoechst positive foci, termed micronuclear tDNA (MN tDNA, Fig. 8A (grey squares)) as they
407 might contain chromosomal DNA fragments with telomeres; and extrachromosomal tDNA
408 without Hoechst stain, termed ex-tDNA. In the following analyses, we focused on the
409 cytoplasmic ex-tDNA (Fig. 8A (yellow squares)). Overall, there were fewer cells with ex-tDNA
410 foci in the HeLa population (7 - 16 %) compared to the U2OS population (36 - 48 %, SFig. 8C).
411 Such a difference is expected for non-ALT cells versus ALT-cells and is consistent with the
412 notion that ex-tDNA foci represent circular ex-tDNAs. Remarkably, both HeLa and U2OS cells
413 mostly contained one ex-tDNA focus per cell for both types of probes (U2OS 25 %, HeLa 5 %),
414 which is strikingly similar to our findings with transfected plasmid DNA ((Wang et al., 2016),
415 Fig. 8B).
416
417 Next, we analyzed whether cytoplasmic ex-tDNA foci are membrane-enclosed in U2OS cells.
418 We could not directly probe for the presence of Emerin, as none of our anti-Emerin antibodies
419 sustained the conditions used in FISH-IF experiments. However, overexpressed Sec61-
420 mCherry colocalized with 47 % of ex-tDNA foci but always colocalized with MN tDNA (Fig. 8C,
421 SFig. 8F). Also, Lap2β was present at 41 % of ex-tDNA foci but always present at MN tDNA
422 foci (Fig. 8D, SFig. 8F). ELYS was never present at ex-tDNA foci but was typically present at
423 MN tDNA (2 out of 3 cases) (Fig. 8E, SFig. 8F). Thus, the co-localization frequencies for the
424 tested ER- and INM-proteins at ex-tDNAs were lower as for plasmid foci, possibly due to the
425 reduced focus size (Fig. 8A,C-E, yellow squares) and the harsh conditions applied during FISH.
426 Notably, NPCs were absent from ex-tDNA but not from tDNA in micronuclei (Fig. 8E, SFig.
427 8F), consistent with the possibility that the latter are formed during mitosis and have different
428 contents than ex-tDNA foci. Collectively, these results indicate that ex-tDNA can also be
429 contained in exclusomes.
430
431

432 **Both plasmid DNA and ex-tDNA cluster in an exclusome**

433 Due to the observed similarities between ex-tDNA and plasmid DNA, we tested if they
434 colocalize within the same exclusomes. U2OS cells were fixed and immunostained for Lap2β
435 24 hours after lipofection with pLacO. In addition, the cells were hybridized *in situ* with probes
436 for both LacO and TelC. Indeed, plasmid and ex-tDNA colocalized in the cytoplasm in one
437 Lap2β containing membrane compartment (Fig. 9A). Among all cells with both types of DNA
438 in the cytoplasm (co-existence cells), 26 % had both DNA types in a single cytoplasmic
439 compartment (Fig. 9B, single exp. SFig. 8G). 75 % of such compartments contained Lap2β in
440 their envelope (Fig. 9A,C, SFig. 8H). In 74 % of such Lap2β-containing compartments plasmid
441 and tDNA foci were Hoechst positive, which could represent chromosomal fragments with
442 telomers together with plasmid DNA (Fig. 9C, SFig. 8H). However, the fact that 26 % of such
443 compartments were Hoechst negative reveals that ex-tDNA, and not telomeric DNA from
444 chromosomal ends, colocalized with plasmid DNA in one cytoplasmic membrane-bound
445 compartment (Fig. 9A). Therefore, we conclude that extra-chromosomal DNAs of different
446 origins, such as endogenous telomeric DNA and exogenous plasmid DNA, can cluster in one
447 exclusome (Fig. 9D).

448 **Discussion**

449

450 Our study reveals that somatic vertebrate cells maintain transfected DNA in a new structure,
451 which we term exclusome and which represents a second cytoplasmic DNA compartment
452 besides the nucleus. The exclusome, mostly one per cell, is a cytoplasmic membranous
453 compartment into which the cell sorts and where it retains transfected plasmid and extra-
454 chromosomal elements, such as telomeric DNA, likely in circular form, for extended periods
455 of time. 24 hours after transfection, the envelope of the exclusome strikingly resembles the
456 nuclear envelope in some aspects but differs from it in others (Fig. 9D). Thus, a nuclear-like
457 envelope was assembled around cytoplasmic plasmid DNA. We observed this in the variety
458 of cells studied here (HeLa, U2OS, MDCK, primary human fibroblasts), suggesting it is not
459 cell type specific amongst somatic cells. This is remarkable, as it enlarges our understanding
460 of the formation of the nucleus and the nuclear envelope.

461

462 The exclusome and the nucleus have three striking similarities. Both contain DNA and exist
463 generally each as a single unit in the cell. In both cases their membranous envelope is a sheet-
464 like double membrane derived from the ER (as shown by the presence of Sec61, LEM4, and
465 KDEL-GFP) and comprising specific INM proteins (Lap2β and Emerin). These points suggest
466 that bringing DNA together in one unit and enwrapping it with a minimal ER-derived double
467 membrane containing Lap2β and Emerin might represent a default response to DNA
468 (Kobayashi et al., 2015).

469

470 However, there are also clear differences distinguishing the exclusome from the nucleus: its
471 envelope structure and its DNA content. The envelope of the exclusome differs from that of
472 the nucleus, as LBR and NPCs are missing, Emerin is enriched, and membrane fenestrations
473 are present in the exclusome envelope but not in the nuclear envelope. At the end of mitosis,
474 Lap2β and Emerin, are known to arrive within the first membrane patches that assemble on
475 the decondensing chromosomes (Haraguchi et al., 2008). In contrast, LBR and NPCs,
476 associate in a second step with the membrane wrapping around the chromosomes (Haraguchi
477 et al., 2000; Lu et al., 2011; Otsuka et al., 2018). Similarly, the sealing of fenestrations does
478 not occur in the envelope of the exclusome however it does occur during the formation of the
479 nuclear envelope late in mitosis (Ventimiglia et al., 2018). Thus earlier, but not later steps of
480 nuclear envelope formation concur to generate the exclusome, which could therefore become
481 a useful model for studying the early events of nuclear envelope assembly.

482

483 Another difference is the enrichment of Emerin in the envelope of the exclusome compared to
484 the nuclear envelope (Haraguchi et al., 2022; Ibrahim et al., 2011; Kobayashi et al., 2015).

485 This hallmark characteristic is in striking contrast to micronuclei, which contain chromosomal
486 fragments or entire chromosomes, as their surrounding membrane is enriched for Lap2β but
487 not for Emerin (Liu et al., 2018). Emerin's enrichment might be due to liberation of Emerin from
488 the INM as seen upon stress (Buchwalter et al., 2019), or is due to accumulation of ER
489 membrane with newly synthesized Emerin at the site of exclusome formation, similarly as seen
490 for the envelopment of chromosomal fragments (Ferrandiz et al., 2022). Our results further
491 suggest that Emerin and its LEM-domain play a key role in the envelopment of plasmid DNA
492 in the cytoplasm. What drives Emerin specificity for exclusomes, in contrast to LEM4 for
493 example, remains to be investigated. Intriguingly the DNA-viruses, vaccinia virus and
494 mimivirus, generate replication factories from the ER in the host cell cytoplasm (Mutsafi et al.,
495 2013; Tolonen et al., 2001). It will be interesting to determine whether the ER at these factories
496 shows similarities to that at the exclusome.
497
498 What do these differences possibly mean? Besides NPCs, we noticed that RCC1 and ELYS
499 were both absent from exclusomes. Both regulate early steps of NPC formation (Gómez-
500 Saldivar et al., 2016; Walther et al., 2003) and their absence might explain why exclusomes
501 do not assemble NPCs. The absence of ELYS would explain that of LBR from exclusomes as
502 well (Mimura et al., 2016). Thus, it will be interesting to determine what causes the absence
503 of ELYS and RCC1 from exclusomes. Possibly, it is due to differences in chromatinization of
504 the DNA in the exclusome compared to that of chromosomes in the nucleus, to which RCC1
505 binds (Chen et al., 2007). Future studies will determine the molecular determinants governing
506 how a given DNA molecule is enveloped and thus how the cell distinguishes extra-
507 chromosomal DNA like plasmid and ex-tDNA from the chromosomes.
508
509 The content of the exclusome differs from that of the nucleus. We reveal processes, by which
510 the cell actively separates chromosomal from extra-chromosomal DNA. The cell sorts
511 transfected plasmid DNA and ex-tDNA into the exclusome, whereas it bundles the
512 chromosomes into the nucleus at the end of mitosis. We show that sorting of incoming plasmid
513 DNA likely occurs directly in the cytoplasm, as most plasmid foci are formed in this
514 compartment. Thereby, only little plasmid DNA reached the nucleus under our transfection
515 and visualization conditions. In this regard, the exclusome prevented contact between the
516 transfected DNA and the chromosomal DNA. When the transfected DNA reached the nucleus,
517 it did not remain there, but was expelled. We identified two modalities by which nuclear
518 plasmids became separated from chromosomal DNA. The first one, mitotic sorting, expels
519 plasmid DNA to the cytoplasm during mitosis. This mechanism was also reported for plasmid
520 DNA microinjected into the nucleus (Ludtke et al., 2002). The second one occurs during
521 interphase and involves the budding of a newly formed exclusome out of the nuclear envelope,

522 into the cytoplasm. Similar, chromosome-derived large circular DNAs encoding c-myc
523 visualized by FISH localized in nuclear buds in the human colorectal adenocarcinoma cancer
524 cell line COLO 320DM (Shimizu et al., 1998). In all cases, the transfected DNA and even
525 originally nuclear ex-tDNA end up in a cytoplasmic exclusome. Thus, the cell has a machinery
526 distinguishing and sorting these DNAs from chromosomal DNA.
527
528 Cells maintain an exclusome with plasmid DNA for long periods of time over multiple cell
529 divisions, but the physiological relevance of this is unknown. Generally, cytoplasmic DNA is
530 sensed as a danger signal by the cyclic guanosine monophosphate–adenosine
531 monophosphate synthase (cGAS), which provokes type I interferon production to warn
532 neighboring cells about this rogue DNA. The organismal immune system would subsequently
533 remove such a cell. As cGAS was found at transfected cytoplasmic plasmid DNA, the
534 exclusome might be an immunologically relevant signaling hub until the cell is eliminated
535 (Guey et al., 2020). Additionally, an exclusome might alter the cellular reaction to other
536 incoming DNAs and could explain why transfection or virus infection are less efficient
537 subsequently to a first transfection (Grandjean et al., 2011; Langereis et al., 2015). In such a
538 scenario, we suggest that the exclusome might act as a memory deposit for both systemic
539 and cell-autonomous immunity towards DNA. In line with this, DNA enwrapping seems to be
540 in competition with nucleases, as most of the transfected DNA is likely degraded before being
541 captured in an exclusome (Shimizu et al., 2005). Also, plasmid foci occasionally disappeared
542 over time, indicating that the maintenance of an exclusome is constantly challenged by cellular
543 defense processes.
544
545 To conclude, we identified that cells distinguish, sort, and cluster extra-chromosomal DNAs
546 away from their chromosomes into a membranous compartment in the cytoplasm, the
547 exclusome. The envelope of the exclusome bears some similarities to the nuclear envelope
548 but also differences as it e.g., does not perform the NPC-controlled nucleo-cytoplasmic
549 exchange of the nuclear envelope. Remarkably, most exclusomes form in interphase cells,
550 whereas the nucleus of mammalian cells forms specifically at mitotic exit. This suggests that
551 DNA clustering and the steps of nuclear envelope formation that are common to the
552 exclusome and the nucleus are not dependent on cell cycle regulation. We suggest that they
553 may have evolved together with open mitosis as a mechanism to exclude extra-chromosomal
554 DNA from the nucleus. Indeed, following transfected plasmid DNA in budding yeast,
555 undergoing closed mitosis, revealed that exclusomes are not present (Denoth-Lippuner et al.,
556 2014; Shcheprova et al., 2008). Still, is the exclusome biology conserved in other, especially
557 non-vertebrate, organisms? We expect it to be especially prominent in organisms undergoing
558 open mitosis and in which cGAS or an analogous system is present.

559 **Material and methods**

560

561 **1. Mammalian cell lines**

562 All cell lines listed in the following were cultured at 37 °C with 5 % CO_2 in a humidified incubator
563 in the indicated media.

564

565 **1.1. HeLa**

566 HeLa Kyoto (HeLa K) (internal Lab ID: MMC278), human cervical cancer cells were a kind gift
567 from P. Meraldi (ETHZ, Switzerland) and originated from S. Narumiya, (Kyoto University,
568 Japan). Cells were cultured in Dulbecco's modified medium (DMEM) with high glucose (Gibco;
569 Thermo Fisher Scientific, Basel, Switzerland) plus 10 % FCS (PAA Laboratories; Pasching,
570 Austria) and P/S (100 U/ml penicillin and 100 mg/ml streptomycin; Gibco, Thermo Fisher
571 Scientific). Results with HeLa K are shown in Fig. 8A,B, SFig. 8A,C.
572 HeLa K cells stably expressing a mutant form of LacI that cannot tetramerize in the fusion
573 proteins LacI-NLS-mCherry (internal Lab ID: MMC114) and LacI-NLS-EGFP (EGFP,
574 enhanced GFP, internal Lab ID: MMC105) were described in (Wang et al., 2016). Cells were
575 cultured as Hela K cells, but the medium contained in addition 5 µg/ml Blasticidine S (Gibco).
576 Both LacI-NLS-XFP cell lines, as well as HeLa transiently expressing LacI-mCherry are
577 referred to "HeLa-LacI" throughout the result and legend text. Results with HeLa LacI-NLS-
578 EGFP are shown in Fig. 2A,C, Fig. 3B, SFig. 1, SFig. 4, SFig. 5C,E,F. Results with HeLa LacI-
579 NLS-mCherry are shown in Fig. 2B, Fig. 3A,C, Fig. 4A-D, Fig. 7, SFig. 1, SFig. 7. HeLa K cells
580 transiently expressing LacI-mCherry were used in Fig. 4E-G, Fig. 5.
581 HeLa K cells stably expressing LacI-NLS-EGFP which were in addition MOCK electroporated,
582 is termed "Control HeLa" (internal Lab ID: MMC248) in SFig.1 but otherwise "HeLa-LacI" to
583 facilitate readability. Cells were cultured like HeLa K cells, but the medium contained
584 additionally 5 µg/ml Blasticidine S (Gibco). Results with this cell line are shown in Fig. 1, SFig.
585 1, SFig. 2, SFig 3.
586 HeLa K cells stably expressing aa 244–453 of Lap2β-GFP (internal Lab ID: MMC84), were
587 kindly provided by U. Kutay and originated from (Mühlhäusser & Kutay, 2007). Results with
588 this cell line are shown in Fig. 5. Expressed aa 244–453 of Lap2β-GFP is termed "Lap2β".

589

590 **1.2. MDCK**

591 MDCK II (Madin-Darby canine kidney) cells stably expressing LacI-NLS-EGFP (internal Lab
592 ID: MMC100), hereafter termed MDCK-LacI, were described in (Wang et al., 2016). Results
593 with this cell line are shown in SFig. 5A-C.

594

595

596 **1.3. U2OS**

597 U2OS osteosarcoma cells (internal Lab ID: MMC95), were a kind gift from C. Azzalin (Instituto
598 de Medicina Molecular, Portugal, cells originated from A. Londono Vallejo). Cells were cultured
599 in Dulbecco's modified medium (DMEM) with high glucose (Gibco) plus 10 % FCS (PAA
600 Laboratories), P/S (Gibco). Results with this cell line are shown in Fig. 8, Fig. 9, SFig. 8B-H.
601

602 **1.4. Primary human fibroblasts**

603 Human primary foreskin fibroblasts (internal Lab ID: MMC281) were kindly provided by Dr.
604 Hans-Dietmar Beer, University of Zurich, Switzerland. The foreskin had been collected with
605 informed written consent of the parents in the context of the Biobank project of the Department
606 of Dermatology, University of Zurich, and its use had been approved by the local and cantonal
607 Research Ethics Committees. Cells were cultured in Dulbecco's modified medium (DMEM)
608 with high glucose (Gibco) plus 10 % FCS (PAA Laboratories) and P/S (Gibco). Results with
609 these cells used at passage number 6 and 7 are shown in Fig. 6, SFig. 5C-F.
610

611 **1.5. Cell cycle synchronization**

612 HeLa cells were synchronized using a double thymidine (2 mM, Sigma Aldrich; St. Lewis,
613 Missouri) treatment. Cells were treated with thymidine for 16 hours, released for 8 hours and
614 treated with thymidine a second time for 20 hours. 1 hour after the second thymidine release,
615 pLacO transfection was performed. 6 hours after pLacO transfection cells were washed with
616 20 U/ml heparin in PBS (3 x 3 min, 37°C). This procedure was used in: Fig. 2A,B, Fig. 3B,D,
617 Fig. 4B-E, Fig. 5.

618 In a second thymidine treatment protocol, cells were treated with thymidine (2 mM, Sigma
619 Aldrich) for 16 hours, then released for 8 hours. 1 hour after this release, plasmids (GFP, GFP-
620 LEM) were lipofected. Cells were exposed to a second thymidine treatment (2 mM) for 18
621 hours. Cells were electroporated with pLacO 2 hours after the second thymidine release. This
622 procedure was used in Fig. 7 and SFig. 7.

623 **2. Plasmid**

624 **2.1. Oligonucleotides used**

internal Lab ID	Sequence 5'-3'
OLIGO273	CCCAAGCTTCTGATTCTGTGGATAACCGTATTAC
OLIGO274	TCCCCCGGGTAAGATACATTGATGAGTTTGG
OLIGO320	GGAATTCCCATGACAACCTCCCAAAAG
OLIGO309	GGTGGATCCCTACAAGAAG
OLIGO328	CTAGCTAGCATGGTGAACGTGAAGC
OLIGO329	CGGGGATCCCAGGCTGCTTCTGGACACCT
OLIGO330	CAGCCATGCTGGTGGCCA

625

626 **2.2. Plasmid preparation**

627 Plasmid DNA was extracted from *E. coli* bacteria (XL1Blue strain or DH5α strain) using
628 plasmid extraction kits (QIAGEN; Venlo, Netherlands or Macherey Nagel; Düren, Germany).
629 The DNA was purified using either Phenol/Chloroform/Isopropanol, ethanol, or 2-Propanol
630 purification. The purified DNA pellet was resuspended in ddH_2O of appropriate volume.
631 Plasmid concentration was measured by a NanoDrop Spectrophotometer (Thermo Fisher
632 Scientific).

633

634 **2.3. Construction of plasmids**

635 pControl 1 is also termed pSR9vector-CMV-mCherry (internal Lab ID: PLA1036): CMV-
636 mCherry-SV40-PA was amplified via PCR and the OLIGO273 and OLIGO274 from p-
637 mCherry-N1 without multiple cloning site (modified Clontech, Takara; United States. Internal
638 Lab ID: PLA1029). The PCR product for CMV-mCherry was cloned into the backbone of
639 pLacO (internal Lab ID: PLA977), after removing the LacO repeats.

640 pLacI-mCherry (no NLS) (internal Lab ID: PLA1107): LacI was amplified with PCR from LacI-
641 NLS-mEGFP (internal Lab ID: PLA978) using OLIGO328 and OLIGO329 with restriction sites
642 for NheI and BamHI. The backbone vector pIRESpuro2-FLAG-mCherry (internal Lab ID:
643 PLA768, kindly gifted from Yves Barral (IBC, ETH Zurich, Switzerland)) was digested with
644 NheI and BamHI and LacI PCR insert was ligated. Clones were checked with sequencing
645 using OLIGO330.

646 pEGFP-LEM-nes (internal Lab ID: PLA1098): The sequence of human Emerin's LEM-domain
647 with a nuclear exclusion signal (nes)(GGAATTCCTCCGAAGATATGGACAACTACGCAGATCTTTCG
648 GATACCGAGCTGACCACCTTGCTGCGCCGGTACAACATCCCGCACGGGCCTGTAGTAGGATCAACTCG
649 TAGGCTTTACGAGAAGAAGATCTTCGAGTACGAGACCCAGAGGCGGCGGGCCCGGGATTTAGCCTTGA
650 AATTAGCAGGTCTTGATATCTACCCCGAAGATTAAGCGGCCGCTAAACTAT) (internal Lab ID: SYN2)
651 was ordered from Lifetechnologies AG (Basel, Switzerland) and inserted into a modified
652 version of pEGFP-N1 (internal lab ID: PLA328).

653 pEGFP-BAF (internal Lab ID: PLA1089): BAF was amplified by PCR from pEGFP-HIS-BAF
654 (internal Lab ID: PLA1080; was a kind gift from Tokuko Haraguchi (National Institute of
655 Information and Communications Technology 588-2 Iwaoka, Iwaoka-choNishi-ku, Kobe 651-
656 2492, Japan)) with the primers OLIGO320 and OLIGO309, digested with EcoRI + BamHI, and
657 inserted into pEGFP-HIS-BAF (internal Lab ID: PLA1080).

658

659 **2.4. Plasmids used**

Plasmid	Source	internal Lab ID	Used in
pEGFP-BAF	this study	PLA1089	Fig. 3C,E
pEGFP-C1	Clontech, Takara	PLA240, PLA997	Fig. 4E-G, Fig. 7, SFig. 7B-E
pEGFP-HIS-BAF	T. Haraguchi (Shimi et al., 2004)	PLA1080	Cloning of PLA1089
p-EGFP-IBB	D. Gerlich (Schmitz et al., 2010)	PLA1061	Fig. 4C
p-EGFP-KDEL	A. Helenius (IBC, ETH Zurich, Switzerland)	PLA936	Fig. 2B
pEGFP-LEM-NES	this study	PLA1098	Fig. 7, SFig. 7B-E
pEGFP-N1	Clontech, Takara, USA	PLA328	Cloning of PLA1098
pEGFP-N3-RCC1	Y. Zheng (Li et al., 2003)	PLA1074	Fig. 4D
p-EGFP-POM121	J. Ellenberg (Beaudouin et al., 2002)	PLA1071	Fig. 4B
pIRESpuro2-FLAG-mCherry-LacI	this study	PLA1107	Fig. 4E-G, Fig.5
pIRESpuro2-FLAG-LacI-NLS-mCherry	Y. Barral (IBC, ETH Zurich, Switzerland)	PLA976	Fig. 6, SFig. 6C-F
pLacI-NLS-mEGFP	(Wang et al., 2016)	PLA978	Fig. 6, SFig. 6C-F
pLacO	S. M. Gasser, (Rohner et al., 2008), as in (Wang et al., 2016)	PLA977	Fig. 1-9, SFig. 1-8
p-mCherry-Sec61β	T. Kirchhausen; (Lu et al., 2009)	PLA948	Fig. 2A, Fig. 8C
p-mCherry-N1 without multiple cloning site	modified from Clontech, Takara, USA		Cloning of PLA1036
pMLBAD (pControl2)	A. Nägeli (Lefebre & Valvano, 2002)	PLA1069	SFig. 5D-F
pSR9vector-CMV-mCherry (pControl1)	this study	PLA1036	SFig. 5D-F

660

661

662

663 **2.5. Plasmid transfection**

664 **Lipofection:** Plasmid was lipofected into cells using X-tremeGENE 9 DNA Transfection
665 Reagent (Roche; Basel, Switzerland). The plasmid:transfection reagent ratio (w:v) was 1:3.
666 Plasmid DNA concentration was either 25 ng (Fig. 2A,B, Fig. 3, Fig. 4, Fig. 5, Fig. 8, Fig. 9,
667 SFig. 8, SFig. 5C HeLa, E,F), 100 ng (Fig. 1, Fig. 2C, Fig. 6A-D, Fig. 7, SFig1, SFig. 2, SFig.
668 3, , SFig. 5, SFig. 6A, SFig. 7, ,), or 330 ng (SFig. 5 MDCK part) per cm^2 cell culture dish area.
669 For double transfections (Fig. 4E-G, Fig. 6, SFig. 6C-F) plasmids were mixed in a 1: 1 ration
670 and transfected at total 100 ng/cm^2 cell culture dish area. To wash away excess transfection
671 mix cells were washed with 20 U/ml heparin (Sigma Aldrich, Switzerland) 6 hours after
672 lipofection in Fig. 3B-D, Fig. 4A-D, SFig. 6B. In all other condition, the lipofection mix was left
673 to incubate with the cells for the time mentioned.

674 **Electroporation:** Electroporation was conducted by a MicroPorator (AxonLab; Baden,
675 Switzerland) with Neon Transfection system 10 µL Kit (invitrogen; Waltham, Massachusetts,
676 United States). The electroporation parameters were 1000 V, 30 ms and 2 pulses for 10 µl
677 electroporation tips using 250 ng DNA per 10^5 suspension cells in R-buffer. Electroporated
678 cells with same condition were collected in a tube and then seeded on cover slips (SFig. 1B,
679 SFig. 5A,B, Fig. 7, SFig. 7),

680

681 **3. FISH**

682 **3.1. FISH probes**

683 **FISH probes of PNA quality**

probe	5' end fluorescent label	Sequence 5' -3'	Company
TelG	Tamra	TTAGGGTTAGGGTTAGGG	Biosynthesis
TelC	Cy5	CCCTAACCCTAACCCTAA	Panagene
LacO	Alexa 488	GAATTGTGAGCGGATAACAATT	Panagene
scramble	Alexa 488	GGGTAGGAGGTTAGTGTTTTGAGT	Panagene

684 **Other FISH probes** were generated with nick-translation method, with Alexa 568-dUTP
685 (Invitrogen), according to manufacturer's instructions on indicated template DNAs.

686

687 **3.2. DNase I enzyme treatment prior to FISH**

688 U2OS and HeLa K cells were fixed with methanol (Supelco; Bellefonte, Pennsylvania, United
689 States) for 10 min at -20 °C and then washed three times in 1x PBS. Cells were permeabilized
690 with 0.5 % Triton X-100 (Sigma-Aldrich, St. Louis, Missouri, United States) for 10 min, then
691 incubated with 0.5 unit/µl DNase (BioConcept; Allschwil, Switzerland) in 1 x PBS for 2 to 2.5
692 hours at 37 °C.

693

694

695 **3.3. Regular FISH**

696 Method modified from (Lansdorp et al., 1996). Cells were rinsed briefly in PBS before fixation.
697 The cells were fixed in 2 % paraformaldehyde (Polyscience; Hirschberg an der Bergstrasse,
698 Germany) in 1x PBS pH 7.4 for 10 min at room temperature (RT) or in 100 % methanol for 10
699 min at -20 °C. Cells were rinsed in 1x PBS three times for 5 min and fixed again for 10 min in
700 methanol at -20 °C if they were fixed with 2 % PFA before. Cells were permeabilized with 0.2
701 % Triton X-100 for 10 or 20 min, then treated with PBS containing 20 mg/ml RNase (Thermo
702 Fisher Scientific) at 37 °C for 30 min to 1 h. PNA probes were diluted to 20 nM concentration
703 in hybridization solution (70 % deionized formamide (Eurobio; Paris, France), 0.5 % blocking
704 reagent (Roche), 10 mM Tris-HCl (pH 7.2)). The DNA was denatured at 80 °C for 3 or 15 min.
705 And then incubated in a humid chamber in the dark for 2 hours at RT. Cells were washed with
706 hybridization wash solution 1 (10 mM Tris-HCl (pH 7.2), 70 % formamide and 0.1 % BSA
707 (Gerbu; Gaiberg, Germany)) for two times, 15 min each time at RT and with hybridization wash
708 solution 2 (100 mM Tris-HCl (pH 7.2), 0.15 M NaCl and 0.08 % Tween-20 (Sigma-Aldrich))
709 for three times. The nuclei were stained by Hoechst33342 (Thermo Fisher Scientific) for 3 min
710 at RT in 1 x PBS and rinsed once with 1x PBS. Cover slips containing cells were mounted in
711 Mowiol 4-88 (Sigma Aldrich) containing 1.4 % w/v DABCO (Sigma Aldrich), sealed with nail
712 polish. This method was applied for the results shown in Fig. 8A,B, SFig. 5E,F, SFig. 8 A-E.

713 **3.4. IF-FISH**

714 After the RNase treatment, cells were blocked with 5 % BSA in 1 x PBST for 1 hour at RT.
715 Then cells were incubated in primary antibody diluted in 1% BSA in 1 x PBST in a humidified
716 chamber for 1 hour at RT. Incubation with the secondary antibody (1:500 for each) in 1 % BSA
717 / 1 x PBST for 1 hour at RT in the dark. Cells were fixed with 4 % paraformaldehyde for 7 min,
718 and then PFA was quenched with 5 % BSA in 1 x PBS and 20 mM glycine for 30 min. Cells
719 were hybridized with probes as described above. This method was applied for the results
720 shown in Fig. 8C,E, Fig. 9, SFig. 8F-H.
721
722
723
724
725
726
727
728
729
730

731 **4. Immunofluorescence**

732 **4.1. Antibodies used**

Antibodies	Source	host	fixation	dilution	Identifier	internal Lab ID
monoclonal NPC (Mab414)	Abcam	mouse	MeOH	1:1000 (U2OS) or 1:2000 (HeLa)	ab24609	AB324
Lap2β	BD transduction laboratories	mouse	formaldehyde	1:500	611000; 27/LAP2	AB273
polyclonal Emerin	Abcam	rabbit	formaldehyde	1:500	ab40688	AB286AB321
serum LEM4	Ian Mattaj, (Asencio et al., 2012)	rabbit	formaldehyde	1:1000	BCFED3 20.1.10	AB282
polyclonal LBR	abcam	rabbit	MeOH		ab122919	AB264
serum ELYS/MEL-28	Iain Mattaj (Franz et al., 2007)	rabbit	formaldehyde	1:200	N/A	AB304
IgG, Alexa-Fluor™ 647	ThermoFischer Scientific	mouse	-	1:500	A21236	AB251
IgG, Alexa-Fluor™ 594	ThermoFischer Scientific	mouse	-	1:500	A11032	AB250
IgG, Alexa-Fluor™ 647	ThermoFischer Scientific	rabbit	-	1:500	A21245	AB316
IgG, Alexa-Fluor™ 594	ThermoFischer Scientific	rabbit	-	1:500	A11037	N/A
IgG, Alexa-Fluor™ 488	ThermoFischer Scientific	rabbit	-	1:500	A11034	AB252

733

734 **4.2 Immunofluorescence staining**

735 Cells in Fig. 3B were fixed 30 hours after pLacO transfection. Cells were either fixed with
736 methanol at -20 °C for 6 min, or with 1 % or 4 % paraformaldehyde for 10 min at RT. Cells
737 were permeabilized for 5 min or 10 min with 0.2 % or 0.1 % TritonX-100 at RT. Blocking was
738 performed with 5 % Bovine serum albumin (Boehringer Mannheim, now Roche) in 1x PBST
739 (1x PBS with 0.05 % Tween-20) for 1 hour at RT. Cells were then incubated with primary
740 antibodies diluted in blocking buffer for 1 hour. Followed by incubation with secondary
741 antibodies diluted in blocking buffer for 45 min to 1 hour. Cells were then stained with 2 µM
742 Hoechst33342 (Molecular probes, Thermo Fisher Scientific) for 10 min and mounted in Mowiol
743 with 1.4 % w/v DABCO. Cover slips were sealed with Nail polish (Lucerna Chem AG; Luzern,
744 Switzerland) and stored at 4 °C.

745

746 **5. Image acquisition**

747 Imaging was done at the Scientific Center for Optical and Electron Microscopy (ScopeM, ETH
748 Zurich).

749

750 **5.1. Fixed cell imaging**

751 For images of fixed cells, z-stacks minimally encompassing entire cells were acquired in 0.3
752 µm or 0.2 µm steps using a 60x NA 1.42 objective on a DeltaVision personalDV multiplexed
753 system (epifluorescence based IX71 (inverse) microscope; Olympus; Tokio, Japan) equipped
754 with a CoolSNAP HQ camera (Roper Scientific; Planegg, Germany).
755 Results shown in Fig. 7, SFig. 7 employed imaging using the DeltaVision personalDV
756 multiplexed system with a 60 x 1.42NA DIC Oil PlanApo Objective and a pco.edge 5.5 camera.
757 Z-stacks were acquired with 0.3 µm steps.
758 A Nikon Wide Field microscope (Nikon Ti2-E; Nikon, Tokio, Japan) was used in Fig. 1A-D,
759 SFig. 1, SFig. 2, SFig. 3 with the S Fluor 20x NA 0.75 DIC N2 WD 1.0mm. For Fig. 6 and SFig.
760 6F, Plan Apo lambda 60x NA 1.4 oil WD 0.13mm was used. Z-stacks with 41 slices x 0.3 um
761 (12 mm total) were acquired, Dapi (Hoechst, DNA) channel was used as reference and the
762 chromatic offset in mCherry and GFP channels was corrected for.
763

764 **5.2. Live-cell microscopy**

765 For live-cell microscopy, three cell lines were used: Control HeLa, HeLa-LacI, or HeLa K cells
766 stably expressing aa 244–453 of Lap2β-GFP transiently overexpressing LacI-mcherry.
767 For results displayed in Fig. 1E,F, Fig. 2A,B, Fig. 3C, Fig. 5, SFig. 4 cells were seeded on Lab-
768 Tek II chambers (Nunc, Thermo Scientific) with CO_2-independent media (Gibco) containing
769 10 % FCS and incubated at a 37 °C on a Spinning Disk microscope (Nipkow spinning disk
770 setup with Nikon Eclipse T1 (inverse) microscope, equipped with 2x EMCCD Andor iXon Ultra
771 cameras, LUDL BioPrecision2 stage with Piezo Focus, Carl Zeiss Microscopy; Jena,
772 Germany). For imaging in Fig. 5 the GFP-Like (Em 520/35) and DsRed-like (Em 617/73)
773 Emission Filter Wheels and 2x Evolve 512 cameras (Photometrics; Tucson, Arizona, United
774 States) were used. For long-term time-lapse imaging (Fig. 5, SFig. 4), cells were recorded
775 every 15 min in z-stacks (33x 0.7 µm steps using a 63x 1.2 NA objective). To monitor cell
776 contours, cells were illuminated with transmission light with single z-focus. For some still
777 images cells expressing Sec61-mCherry (Fig. 2A), eGFP-KDEL (Fig. 2B) and eGFP-BAF (Fig.
778 3C) were imaged after incubation with 2 µM Hoechst33342 for 10 min, using a DeltaVision
779 microscope (DeltaVision personalDV system (epifluorescence based IX71 (inverse)
780 microscope; Olympus).
781 For results displayed in Fig. 1, SFig. 2, SFig. 3, HeLa Control cells were seeded on ibidi 8-well
782 chambers (ibidi µ-Slide 8 well ibiTreat, Gräfelfing, Germany). 24 hours after seeding, cells
783 were incubated at 37 °C with 5% CO_2 (OkoLab, Pozzouli NA, Italy) either at the Visitron
784 Spinning Disk (experiments e1 (internal Lab ID: EXP345) and e2 (internal Lab ID: EXP337))
785 or a Nikon Wide Field microscope (Nikon Ti2-E (inverse), experiments e3 and e4 (internal Lab
786 ID: EXP604)). For Visitron spinning disk imaging a GFP-Like (Em 520/35) Emission Filter

787 Wheel and 2x Evolve 512 cameras (Photometrics) were used. Bright field imaging was done
788 with the coolLED *p*E-100 control system (coolLED; Andover, Great Britain). For Nikon Wide
789 Field imaging the GFP (Em 515/30) Emission Filter Wheel or bright field pre-setting was used.
790 For detection, the Orca Fusion BT (Hamamatsu; Shizuoka, Japan) (2304x2304 pixels, 6.5 µm
791 x 6.5 µm) system was used. For each experiment at the Visitron Spinning Disk microscope, 5
792 regions of interest (ROI) were imaged. For each experiment at the Nikon Wide Field
793 microscope, 6 ROI were imaged. In the live-cell analysis included are only ROI with 0.9766
794 cells/pixel, thus one ROI of e1 at the Visitron Spinning Disk microscope and two ROI of e3 as
795 well as two ROI of e4 at the Nikon Wide Field microscopewere excluded. Cells were recorded
796 every 30 min as z-stacks (22 x 0.7 µm steps using 20x 0.75 CFI Plan Apo VC at the Visitron
797 Spinning disk and 22 x 0.7 µm steps using S Fluor 20 x NA 0.75 DIC N2 WD 1.0mm at the
798 Nikon Wide Field). On both microscopes, cells were lipofected with pLacO using X-
799 tremeGENE 9 DNA Transfection Reagent (Roche). The plasmid:transfection reagent ratio
800 (w:v) was 1:3 with a plasmid DNA concentration of 100 ng/cm^2. The lipofection mix remained
801 on the cells during imaging. The death rate was low at both microscopes (SFig. 2A).
802
803 **5.3. FRAP**
804 FRAP experiments (Fig. 4E-G) were performed using a modified method that was previously
805 reported (Clay et al., 2014). 24 hours after pLacO transfection, live HeLa-LacI cells (seeded
806 on a Lab-TekTM II chamber, CO_2-independent media, 37 °C incubator) and free eGFP were
807 imaged on a confocal microscope (LSM 760; Carl Zeiss Microscopy) with a Plan Apochromat
808 63x /1.4 NA oil immersion objective. The ZEN software (Carl Zeiss Microscopy) was used to
809 control the microscope. eGFP emission was detected with a 505 nm long pass filter.
810 Photobleaching was applied on a region of interest (cluster and then control area) as indicated
811 in Fig. 4E-G. Bleaching was applied with 50-100 iterations using 30-50 % laser power, but
812 always with the same settings between the cluster and control area in each cell.
813
814 **5.4. Correlative light and electron microscopy (CLEM)**
815 HeLa K cells stably expressing LacI-NLS-mCherry were cultured on a 3.5 cm glass bottom
816 dish with grid (MatTek; Ashland, Massachusetts, United States) and transfected with pLacO
817 for 24 hours. Cells were processed as described in (Wang et al., 2016).
818
819 **6. Data Analysis (Fiji, Prism, Diatrack, etc.)**
820 **6.1. Image processing**
821 Images acquired from DeltaVision (Olympus) microscope (Fig. 2C, Fig. 3B-D, Fig. 4A-D, Fig.
822 8, SFig. 9A, SFig. 5A,E, SFig. 6A, SFig. 7C,D, SFig. 8A,B,D) were deconvolved using
823 Softworx (Applied Precision; Rača, Slowakia). Images acquired from LSM 710 confocal

824 microscope were deconvolved using Huygens Software (Scientific Volume Imaging;
825 Hilversum, Netherlands) before correlating with EM images (Fig. 2A). The correlation analysis
826 between confocal and EM images (Fig. 3A) were performed using Amira software
827 (FEI/Thermo Fisher Scientific), as in (Wang et al., 2016). General, the presented images are
828 single z-slices or if indicated projections of multiple z-slices images.
829 Images in Fig. 3A (confocal image), Fig. 6 and SFig. 6F were deconvolved using Huygens
830 (Scientific Volume Imaging).
831
832 **6.2. Image analyses**
833 Images were analyzed using Fiji 1.51n Software.
834
835 **6.2.1 Colocalization**
836 For co-localization analyses, the overlay of the reporter fluorescence and LacI fluorescence
837 was used (Fig. 2C, Fig. 6, Fig. 8, SFig. 6D,E, SFig. 8). The qualitative classes for reporter
838 molecules “enriched”, “non-enriched”, “present” and “absent” are established applying the
839 following rules:
840
841 For experiments presented in Fig. 3, Fig. 4:
842 Generally, marker fluorescence intensities were used to qualitatively determine co-localization
843 of markers with the plasmid focus with the following criteria.
844 “Non-enriched”: plasmid foci with marker fluorescence signal in the z-stack slice in, directly
845 underneath or above the position of the plasmid focus, and/or marker fluorescence signal in
846 xy-direction adjacent. The intensity of the marker fluorescence is like the cytoplasmic marker
847 fluorescence (relative readout to the intensity of the rest of the cell).
848 Plasmid foci with marker “enriched” have marker fluorescence at same positions described in
849 “non-enriched”, but with higher intensities compared to the reference marker fluorescence of
850 the respective marker (i.e., Emerin at NE or in ER; LEM4 in ER). Where sensible, results state
851 the two “enriched” reference marker fluorescence (i.e., ER or NE).
852 Category “present” (Fig. 8 and Fig. 4) encompasses “enriched” and “non-enriched”.
853 Plasmid foci with marker “absent” do not have marker fluorescence in the adjacent slides,
854 underneath or above the position of the focus, nor a marker fluorescence signal in xy direction
855 adjacent to the focus nor in the sliced with the focus.
856 For data presented in Fig. 3E:
857 For Emerin and Lap2β, the quantitative enrichment factor analysis (below) were back
858 translated into qualitative classification: "enriched” with an enrichment factor >1, or “non-
859 enriched” with 0>enrichment factor>1, or “absent” for enrichment factor being zero. For BAF

860 and LBR, the classification of “enriched”, “non-enriched”, and “absent” as described above for
861 Fig. 3 was used.
862
863 For data presented in Fig. 6, SFig. 6C-F:
864 In the single z-slice, where the plasmid focus was in focus, a line scan across the biggest axis
865 of the plasmid focus and either the ER (for LEM4) or across the nucleus (for Emerin) was
866 made, displaying the intensity distribution along that line (Fiji, line scan). Classification was
867 according to the following intensity criteria: enriched > NE or > ER: the average intensity of
868 the reporter (Emerin or LEM4) at the plasmid focus was higher compared to the average
869 reporter intensity at the NE or surrounding ER, displayed along the line. Like ER: fluorescence
870 of the reporter (Emerin or LEM4) was in average identical the intensity in the ER surrounding
871 the plasmid focus. Absent: no intensity of the reporter (Emerin or LEM4) at the plasmid focus.
872
873 For the experiments presented in Fig. 7:
874 Intensities of reporter proteins (LEM4 or Emerin) at the plasmid focus were visually compared
875 to intensities reporter proteins in the surrounding cytoplasm. “Present”: If the reporter intensity
876 was equal or higher at the plasmid focus than that of the surrounding cytoplasm in the focal
877 slice, directly underneath or above the focus-position of the plasmid focus (0.3 µm distances).
878 Otherwise, the classification was “absent”.
879
880 For the experiments presented in SFig. 7B,C:
881 The intensity of Emerin immunofluorescence was measured as RawIntDen (Fiji) in a square
882 (20x20 px) covering ER and in a same sized square covering the nucleus of a single cells in
883 maximum intensity projected images. Chosen were in both cases regions where the intensity
884 appeared the most intense as judge by eye. The ratio between the RawIntDen value at the
885 NE divided by that at the ER was calculated for each cell with minimally 1 cytoplasmic plasmid
886 focus. A ratio above 1 reports about a higher intensity of Emerin (and therefore more Emerin)
887 at the NE compared to the ER of that same cell. A ratio below 1 represents a higher intensity
888 of Emerin (and therefore more Emerin) at the ER compared to the NE of the same cell.
889
890 Quantitative enrichment factor analysis (SFig. 6B):
891 Single z-slice images were analyzed. The fluorescence intensity was measured along a line
892 crossing the plasmid focus and the nucleus. Along this line, the fluorescent intensities of two
893 brightest pixels at the edges of the plasmid focus (I (c1), I (c2)) or the nucleus (I (n1), I (n2)),
894 were averaged. Another averaged intensity of 30-50 pixels along this line, in a cytoplasmic
895 region, was used as background intensity (I (background)). The enrichment factor was

896 calculated as: (Enrichment factor = ((I(c1)+I (c2))*0.5 - I (background))/ ((I (n1)+I (n2))*0.5 - I
897 (background)).
898
899 **6.2.2 Live-cell imaging analyses**
900 **Plasmid focus localization** (Fig. 1, SFig. 2, SFig. 3):
901 For plasmid focus analyses, two interphase localizations are classified: cytoplasmic and
902 nuclear. Cytoplasmic plasmid foci: These intracellular LacI-positive plasmid foci are outside of
903 the volume marked by LacI-NLS-GFP fluorescence reporting about the nucleus or are at the
904 cytoplasmic side of the nuclear envelope, which is reported by the outer boarder of the nuclear
905 LacI-NLS-GFP fluorescence, but with minimally 1 pixel of background intensity between the
906 LacI intensity at the plasmid focus and that of the nucleus. Plasmid foci in the nucleus are
907 either nucleoplasmic LacI-positive foci or LacI-positive foci at the nucleoplasmic side of the
908 nuclear envelope, which is reported by the outer boarder of nuclear LacI-NLS-GFP
909 fluorescence. Nucleoplasmic plasmid foci (nuclear foci) are defined as plasmid foci inside the
910 volume of nuclear LacI-NLS-GFP fluorescence but with an intensity higher than that of the
911 general nuclear LacI-NLS-GFP fluorescence. In addition, the z-slice in which the plasmid focus
912 is most in focus (focal-z-slice) and at highest intensity is also the z-slice, in which nuclear LacI-
913 NLS-GFP fluorescence covers the biggest area. Further, the focal-z-slice of the plasmid lies
914 in between other z-slices in which the general nuclear LacI-NLS-GFP fluorescence is still in
915 focus. Typically, depending on the z-stack spacing, the general nuclear LacI-NLS-GFP
916 fluorescence is still in focus within +/- 1 µm of the focal plane of the plasmid focus. This is to
917 be compared to a situation, where a plasmid focus is at the nuclear envelope and thus in an
918 upper z-slice. In this case the plasmid focal plane is not identical with the z-slice of the biggest
919 area of general nuclear fluorescence. These classification criteria were used in Fig. 1, SFig.
920 2, SFig. 3 as well as for classification of plasmid foci being formed in the nucleoplasm in SFig.
921 5G+H. We chose these strict conditions to exclude the option of a false positive nuclear
922 assignment to plasmid foci.
923
924 **Origin-destination analysis** (Fig. 1D, SFig. 2H):
925 To avoid analyzing plasmid foci that formed in the cytoplasm but in close proximity to the NE,
926 we excluded plasmid foci that formed at the inner side of the nuclear periphery from the
927 analysis focusing thus on foci formed in the inner nucleoplasm. To allow for sorting time the
928 last 25 % of the forming plasmid foci in the pooled data set were excluded from this analysis.
929 For the “origin-destination” analysis the location of formation of each plasmid focus was noted
930 (“origin”) (either interphase: cytoplasm or nucleoplasm, or during mitosis). Then, after tracing
931 the focus over time until the end of imaging, the location of each plasmid focus at imaging end
932 (“destination”) was noted. If during imaging a cell fused with another cell, died, produced a

933 micronucleus, the nucleus fragmented, the plasmid focus disappeared, or the cell was in
934 mitosis at the end of imaging the focus localization in the last frame before one of these events
935 was noted as the corresponding destination of the given plasmid focus. Only cells that
936 completed a mitosis (first frame with two distinct nuclei in LacI-NLS-GFP channel and two fully
937 divided cells in brightfield channel) were analyzed.
938
939 **FRAP quantification** (Fig. 4E,F):
940 Using Fiji, the mean fluorescence recovery signal was quantified in the bleached area. The
941 fluorescence signal was normalized to that at the beginning of the experiment. All experiments
942 were transferred to Prism software (GraphPad) and fit on an exponential FRAP curve, the
943 mobile fraction was measured by determining the half time ($t_{1/2}$) of fluorescence recovery to
944 reach a plateau level.
945
946 **FISH co-localization analysis** (Fig. 8, Fig. 9, SFig. 8):
947 Fluorescence signals of stained proteins were boosted until the background level of the cell's
948 cytoplasm was visible. Proteins co-localized at telomeric DNA if the signals at the telomeric
949 DNA foci were visually than the background in close vicinity and the boosted setting.
950
951 **7. Statistics**
952 Statistics were conducted using Prism 8.0.0 (GraphPad) built-in analysis tools, methods used
953 are indicated in the figure legends.
954 Data were tested with Gaussian distribution for normality (*D'Agostino & Pearson* normality test)
955 (α=0.05)) if t-tests were used.
956
957 **Acknowledgements**
958 We thank Yves Barral (ETH-Zürich), for continued discussions and support of this study. We
959 thank Madhav Jagannathan, members of the Kroschewski and Barral labs for helpful
960 discussions and comments on the manuscript. We acknowledge financial support by Swiss
961 National Science Foundation (grant 31003A_172908/1 to RK) and the Novartis foundation for
962 medical-biological research (grant 20C229 to RK).
963
964 **Competing interest**
965 The authors declare no conflict of interest
966
967
968
969

References

Anderson, D. J., & Hetzer, M. W. (2008). Reshaping of the endoplasmic reticulum limits the rate for nuclear envelope formation. *The Journal of Cell Biology*, *182*(5), 911-924. https://doi.org/10.1083/jcb.200805140 PMID - 18779370

Asencio, C., Davidson, I. F., Santarella-Mellwig, R., Ly-Hartig, T. B. N., Mall, M., Wallenfang, M. R., Mattaj, I. W., & Gorjánácz, M. (2012). Coordination of kinase and phosphatase activities by Lem4 enables nuclear envelope reassembly during mitosis. *Cell*, *150*(1), 122 - 135. https://doi.org/10.1016/j.cell.2012.04.043

Beaudouin, J., Gerlich, D., Daigle, N., Eils, R., & Ellenberg, J. (2002). Nuclear Envelope Breakdown Proceeds by Microtubule-Induced Tearing of the Lamina. *Cell*, *108*(1), 83-96. https://doi.org/10.1016/s0092-8674(01)00627-4 PMID - 11792323

Buchwalter, A., Schulte, R., Tsai, H., Capitanio, J., & Hetzer, M. (2019). Selective clearance of the inner nuclear membrane protein emerin by vesicular transport during ER stress. *eLife*, *8*. https://doi.org/10.7554/elife.49796

Cesare, A. J., & Griffith, J. D. (2004). Telomeric DNA in ALT cells is characterized by free telomeric circles and heterogeneous t-loops. *Molecular and cellular biology*, *24*(22), 9948 - 9957. https://doi.org/10.1128/mcb.24.22.9948-9957.2004

Chen, T., Muratore, T. L., Schaner-Tooley, C. E., Shabanowitz, J., Hunt, D. F., & Macara, I. G. (2007). N-terminal α-methylation of RCC1 is necessary for stable chromatin association and normal mitosis. *Nature Cell Biology*, *9*(5), 596 - 603. https://doi.org/10.1073/pnas.0402700101

Chen, Y.-A., Shen, Y.-L., Hsia, H.-Y., Tiang, Y.-P., Sung, T.-L., & Chen, L.-Y. (2017). Extrachromosomal telomere repeat DNA is linked to ALT development via cGAS-STING DNA sensing pathway. *Nature structural & molecular biology*, *24*(12), 1124-1131. https://doi.org/10.1038/nsmb.3498

Clay, L., Caudron, F., Denoth-Lippuner, A., Boettcher, B., Buvelot Frei, S., Snapp, E. L., & Barral, Y. (2014). A sphingolipid-dependent diffusion barrier confines ER stress to the yeast mother cell. *eLife*, *3*, e01883. https://doi.org/10.7554/eLife.01883

Crasta, K., Ganem, N. J., Dagher, R., Lantermann, A. B., Ivanova, E. V., Pan, Y., Nezi, L., Protopopov, A., Chowdhury, D., & Pellman, D. (2012). DNA breaks and chromosome pulverization from errors in mitosis. *Nature*, *482*(7383), 53-58. https://doi.org/10.1038/nature10802

Denoth-Lippuner, A., Krzyzanowski, M. K., Stober, C., & Barral, Y. (2014). Role of SAGA in the asymmetric segregation of DNA circles during yeast ageing. *eLife*, *3*, e03790. https://doi.org/10.7554/eLife.03790

Ferrandiz, N., Downie, L., Starling, G. P., & Royle, S. J. (2022). Endomembranes promote chromosome missegregation by ensheathing misaligned chromosomes. *Journal of Cell Biology*, *221*(6), e202203021. https://doi.org/10.1083/jcb.202203021 PMID - 35486148

Franz, C., Walczak, R., Yavuz, S., Santarella, R., Gentzel, M., Askjaer, P., Galy, V., Hetzer, M., Mattaj, I. W., & Antonin, W. (2007). MEL-28/ELYS is required for the recruitment of nucleoporins to chromatin and postmitotic nuclear pore complex assembly. *EMBO Reports*, *8*(2), 165 - 172. https://doi.org/10.1038/sj.embor.7400889

Gerber, T., Loureiro, C., Schramma, N., Chen, S., Jain, A., Weber, A., Weigert, A., Santel, M., Alim, K., Treutlein, B., & Camp, J. G. (2022). Spatial transcriptomic and single-nucleus analysis reveals heterogeneity in a gigantic single-celled syncytium. *eLife*, *11*, e69745. https://doi.org/10.7554/elife.69745 PMID - 35195068

Gómez-Saldivar, G., Fernandez, A., Hirano, Y., Mauro, M., Lai, A., Ayuso, C., Haraguchi, T., Hiraoka, Y., Piano, F., & Askjaer, P. (2016). Identification of Conserved MEL-28/ELYS Domains with Essential Roles in Nuclear Assembly and Chromosome Segregation. *PLoS genetics*, *12*(6), e1006131. https://doi.org/10.1371/journal.pgen.1006131

Grandjean, M., Girod, P.-A., Calabrese, D., Kostyrko, K., Wicht, M., Yerly, F., Mazza, C., Beckmann, J. S., Martinet, D., & Mermod, N. (2011). High-level transgene expression by homologous recombination-mediated gene transfer. *Nucleic Acids Research*, *39*(15), e104-e104. https://doi.org/10.1093/nar/gkr436 PMID - 21652640

Guey, B., Wischnewski, M., Decout, A., Makasheva, K., Kaynak, M., Sakar, M. S., Fierz, B., & Ablasser, A. (2020). BAF restricts cGAS on nuclear DNA to prevent innate immune activation. *Science (New York, NY)*, *369*(6505), 823 - 828. https://doi.org/10.1126/science.aaw6421

Güttinger, S., Laurell, E., & Kutay, U. (2009). Orchestrating nuclear envelope disassembly and reassembly during mitosis. *Nature Reviews Molecular Cell Biology*, *10*(3), 178-191. https://doi.org/10.1038/nrm2641

Haraguchi, T., Kojidani, T., Koujin, T., Shimi, T., Osakada, H., Mori, C., Yamamoto, A., & Hiraoka, Y. (2008). Live cell imaging and electron microscopy reveal dynamic processes of BAF-directed nuclear envelope assembly. *Journal of Cell Science*, *121*(15), 2540-2554. https://doi.org/10.1242/jcs.033597

Haraguchi, T., Koujin, T., Hayakawa, T., Kaneda, T., Tsutsumi, C., Imamoto, N., Akazawa, C., Sukegawa, J., Yoneda, Y., & Hiraoka, Y. (2000). Live fluorescence imaging reveals early recruitment of emerin, LBR, RanBP2, and Nup153 to reforming functional nuclear envelopes. *Journal of Cell Science*, *113*(5), 779-794. https://doi.org/10.1242/jcs.113.5.779

Haraguchi, T., Koujin, T., Segura-Totten, M., Lee, K. K., Matsuoka, Y., Yoneda, Y., Wilson, K. L., & Hiraoka, Y. (2001). BAF is required for emerin assembly into the reforming nuclear envelope. *Journal of Cell Science*, *114*(24), 4575-4585. https://doi.org/10.1242/jcs.114.24.4575

Haraguchi, T., Koujin, T., Shindo, T., Bilir, Ş., Osakada, H., Nishimura, K., Hirano, Y., Asakawa, H., Mori, C., Kobayashi, S., Okada, Y., Chikashige, Y., Fukagawa, T., Shibata, S., & Hiraoka, Y. (2022). Transfected plasmid DNA is incorporated into the nucleus via nuclear envelope reformation at telophase. *Communications Biology*, *5*(1), 78. https://doi.org/10.1038/s42003-022-03021-8

Hatch, Emily M., Fischer, Andrew H., Deerinck, Thomas J., & Hetzer, Martin W. (2013). Catastrophic Nuclear Envelope Collapse in Cancer Cell Micronuclei. *Cell*, *154*(1), 47-60. https://doi.org/https://doi.org/10.1016/j.cell.2013.06.007

Ibrahim, N., Wicklund, A., & Wiebe, M. S. (2011). Molecular characterization of the host defense activity of the barrier to autointegration factor against vaccinia virus. *J Virol*, *85*(22), 11588–11600. https://doi.org/10.1128/JVI.00641-11

Karg, T., Warecki, B., & Sullivan, W. (2015). Aurora B–mediated localized delays in nuclear envelope formation facilitate inclusion of late-segregating chromosome fragments. *Molecular biology of the cell*, *26*(12), 2227-2241. https://doi.org/10.1091/mbc.e15-01-0026 PMID - 25877868

Kneissig, M., Keuper, K., Pagter, M. S. d., Roosmalen, M. J. v., Martin, J., Otto, H., Passerini, V., Sparr, A. C., Renkens, I., Kropveld, F., Vasudevan, A., Sheltzer, J. M., Kloosterman, W. P., & Storchova, Z. (2019). Micronuclei-based model system reveals functional consequences of chromothripsis in human cells. *eLife*, *8*, e50292. https://doi.org/10.7554/elife.50292 PMID - 31778112

Kobayashi, S., Koujin, T., Kojidani, T., Osakada, H., Mori, C., Hiraoka, Y., & Haraguchi, T. (2015). BAF is a cytosolic DNA sensor that leads to exogenous DNA avoiding autophagy. *Proceedings of the National Academy of Sciences of the United States of America*, *112*(22), 7027–7032. https://doi.org/10.1073/pnas.1501235112

Kopesky, P., Tiedemann, K., Alkekhia, D., Zechner, C., Millard, B., Schoeberl, B., & Komarova, S. V. (2014). Autocrine signaling is a key regulatory element during osteoclastogenesis. *Biology Open*, *3*(8), 767-776. https://doi.org/10.1242/bio.20148128 PMID - 25063197

Langereis, M. A., Rabouw, H. H., Holwerda, M., Visser, L. J., & Kuppeveld, F. J. M. v. (2015). Knockout of cGAS and STING Rescues Virus Infection of Plasmid DNA-Transfected Cells. *J Virol*, *89*(21), 11169 - 11173. https://doi.org/10.1128/jvi.01781-15

Lansdorp, P. M., Verwoerd, N. P., Rijke, F. M. v. d., Dragowska, V., Little, M.-T., Dirks, R. W., Raap, A. K., & Tanke, H. J. (1996). Heterogeneity in Telomere Length of Human Chromosomes. *Human Molecular Genetics*, *5*(5), 685-691. https://doi.org/10.1093/hmg/5.5.685 PMID - 8733138

Lee, K. K., Haraguchi, T., Lee, R. S., Koujin, T., Hiraoka, Y., & Wilson, K. L. (2001). Distinct functional domains in emerin bind lamin A and DNA-bridging protein BAF. *Journal of Cell Science*, *114*(24), 4567 - 4573. http://www.ncbi.nlm.nih.gov/pubmed/11792821

Lefebre, M. D., & Valvano, M. A. (2002). Construction and Evaluation of Plasmid Vectors Optimized for Constitutive and Regulated Gene Expression in Burkholderia cepacia Complex Isolates. *Applied and Environmental Microbiology*, *68*(12), 5956-5964. https://doi.org/10.1128/aem.68.12.5956-5964.2002 PMID - 12450816

Li, H. Y., Wirtz, D., & Zheng, Y. (2003). A mechanism of coupling RCC1 mobility to RanGTP production on the chromatin in vivo. *Journal of Cell Biology*, *160*(5), 635-644. https://doi.org/10.1083/jcb.200211004

Liu, S., Kwon, M., Mannino, M., Yang, N., Renda, F., Khodjakov, A., & Pellman, D. (2018). Nuclear envelope assembly defects link mitotic errors to chromothripsis. *Nature*, *561*(7724), 551-555. https://doi.org/10.1038/s41586-018-0534-z

Lu, L., Ladinsky, M. S., & Kirchhausen, T. (2009). Cisternal organization of the endoplasmic reticulum during mitosis. *Molecular biology of the cell*, *20*(15), 3471 - 3480. https://doi.org/10.1091/mbc.e09-04-0327

Lu, L., Ladinsky, M. S., & Kirchhausen, T. (2011). Formation of the postmitotic nuclear envelope from extended ER cisternae precedes nuclear pore assembly. *Journal of Cell Biology*, *194*(3), 425-440. https://doi.org/10.1083/jcb.201012063

Ludtke, J. J., Sebestyén, M. G., & Wolff, J. A. (2002). The Effect of Cell Division on the Cellular Dynamics of Microinjected DNA and Dextran. *Molecular Therapy*, *5*(5), 579-588. https://doi.org/https://doi.org/10.1006/mthe.2002.0581

Mimura, Y., Takagi, M., Clever, M., & Imamoto, N. (2016). ELYS regulates the localization of LBR by modulating its phosphorylation state. *Journal of Cell Science*, *129*(22), 4200-4212. https://doi.org/10.1242/jcs.190678 PMID - 27802161

Mühlhäusser, P., & Kutay, U. (2007). An in vitro nuclear disassembly system reveals a role for the RanGTPase system and microtubule-dependent steps in nuclear envelope breakdown. *The Journal of Cell Biology*, *178*(4), 595 - 610. https://doi.org/10.1083/jcb.200703002

Mutsafi, Y., Shimoni, E., Shimon, A., & Minsky, A. (2013). Membrane Assembly during the Infection Cycle of the Giant Mimivirus. *PLoS Pathogens*, *9*(5), e1003367. https://doi.org/10.1371/journal.ppat.1003367

Noer, J. B., Hørsdal, O. K., Xiang, X., Luo, Y., & Regenberg, B. (2022). Extrachromosomal circular DNA in cancer: history, current knowledge, and methods. *Trends in Genetics*, *38*(7), 766-781. https://doi.org/https://doi.org/10.1016/j.tig.2022.02.007

Orr, B., Sousa, F. D., Gomes, A. M., Afonso, O., Ferreira, L. T., Figueiredo, A. C., & Maiato, H. (2021). An anaphase surveillance mechanism prevents micronuclei formation from frequent chromosome segregation errors. *Cell Reports*, *37*(6), 109783. https://doi.org/10.1016/j.celrep.2021.109783 PMID - 34758324

Otsuka, S., Steyer, A. M., Schorb, M., Hériché, J.-K., Hossain, M. J., Sethi, S., Kueblbeck, M., Schwab, Y., Beck, M., & Ellenberg, J. (2018). Postmitotic nuclear pore assembly proceeds by radial dilation of small membrane openings. *Nature structural & molecular biology*, *25*(1), 21-28. https://doi.org/10.1038/s41594-017-0001-9

Paulsen, T., Kumar, P., Koseoglu, M. M., & Dutta, A. (2018). Discoveries of Extrachromosomal Circles of DNA in Normal and Tumor Cells. *Trends in Genetics*, *34*(4), 270 - 278. https://doi.org/10.1016/j.tig.2017.12.010

Rasala, B. A., Orjalo, A. V., Shen, Z., Briggs, S., & Forbes, D. J. (2006). ELYS is a dual nucleoporin/kinetochore protein required for nuclear pore assembly and proper cell division. *Proceedings of the National Academy of Sciences of the United States of America*, *103*(47), 17801-17806. https://doi.org/10.1073/pnas.0608484103

Regev, A., Cohen, S., Cohen, E., Bar-Am, I., & Lavi, S. (1999). Telomeric repeats on small polydisperse circular DNA (spcDNA) and genomic instability. *Oncogene*, *17*(26), 3455 - 3461. https://doi.org/doi:10.1038/sj.onc.1202250

Rohner, S., Gasser, S. M., & Meister, P. (2008). Modules for cloning-free chromatin tagging in Saccharomyces cerevisae. *Yeast*, *25*(3), 235 - 239. https://doi.org/10.1002/yea.1580

Samwer, M., Schneider, M. W. G., Hoefler, R., Schmalhorst, P. S., Jude, J. G., Zuber, J., & Gerlich, D. W. (2017). DNA Cross-Bridging Shapes a Single Nucleus from a Set of Mitotic Chromosomes. *Cell*, *170*(5), 956 - 972.e923. https://doi.org/10.1016/j.cell.2017.07.038

Schmitz, M. H. A., Held, M., Janssens, V., Hutchins, J. R. A., Hudecz, O., Ivanova, E., Goris, J., Trinkle-Mulcahy, L., Lamond, A. I., Poser, I., Hyman, A. A., Mechtler, K., Peters, J.-M., & Gerlich, D. W. (2010). Live-cell imaging RNAi screen identifies PP2A–B55α and importin-β1 as key mitotic exit regulators in human cells. *Nature Cell Biology*, *12*(9), 886-893. https://doi.org/10.1038/ncb2092 PMID - 20711181

Shcheprova, Z., Baldi, S., Frei, S. B., Gonnet, G., & Barral, Y. (2008). A mechanism for asymmetric segregation of age during yeast budding. *Nature*, *454*(7205), 728-734. https://doi.org/10.1038/nature07212

Shimi, T., Koujin, T., Segura-Totten, M., Wilson, K. L., Haraguchi, T., & Hiraoka, Y. (2004). Dynamic interaction between BAF and emerin revealed by FRAP, FLIP, and FRET analyses in living HeLa cells. *Journal of Structural Biology*, *147*(1), 31 - 41. https://doi.org/10.1016/j.jsb.2003.11.013

Shimizu, N., Itho, N., Utiyama, H., & Wahl, G. M. (1998). Selective Entrapment of Extrachromosomally Amplified DNA by Nuclear Budding and Micronucleation during S Phase. *The Journal of Cell Biology*, *140*(6), 1307 - 1320. https://doi.org/10.1083/jcb.140.6.1307

Shimizu, N., Kamezaki, F., & Shigematsu, S. (2005). Tracking of microinjected DNA in live cells reveals the intracellular behavior and elimination of extrachromosomal genetic material. *Nucleic Acids Research*, *33*(19), 6296 - 6307. https://doi.org/10.1093/nar/gki946

Tokutake, Y., Matsumoto, T., Watanabe, T., Maeda, S., Tahara, H., Sakamoto, S., Niida, H., Sugimoto, M., Ide, T., & Furuichi, Y. (1998). Extra-Chromosomal Telomere Repeat DNA in Telomerase-Negative Immortalized Cell Lines. *Biochemical and biophysical research communications*, *247*(3), 765-772. https://doi.org/https://doi.org/10.1006/bbrc.1998.8876

Tolonen, N., Doglio, L., Schleich, S., & Locker, J. K. (2001). Vaccinia Virus DNA Replication Occurs in Endoplasmic Reticulum-enclosed Cytoplasmic Mini-Nuclei. *Molecular biology of the cell*, *12*(7), 2031-2046. https://doi.org/10.1091/mbc.12.7.2031 PMID - 11452001

Ventimiglia, L. N., Cuesta-Geijo, M. A., Martinelli, N., Caballe, A., Macheboeuf, P., Miguet, N., Parnham, I. M., Olmos, Y., Carlton, J. G., Weissenhorn, W., & Martin-Serrano, J. (2018). CC2D1B Coordinates ESCRT-III Activity during the Mitotic Reformation of the Nuclear Envelope. *Developmental Cell*, *47*(5), 547-563.e546. https://doi.org/10.1016/j.devcel.2018.11.012 PMID - 30513301

Vidaček, N. Š., Ćukušić, A., Ivanković, M., Fulgosi, H., Huzak, M., Smith, J. R., & Rubelj, I. (2010). Abrupt telomere shortening in normal human fibroblasts. *Experimental Gerontology*, *45*(3), 235-242. https://doi.org/10.1016/j.exger.2010.01.009 PMID - 20080170

Walther, T. C., Askjaer, P., Gentzel, M., Habermann, A., Griffiths, G., Wilm, M., Mattaj, I. W., & Hetzer, M. (2003). RanGTP mediates nuclear pore complex assembly. *Nature*, *424*(6949), 689 - 694. https://doi.org/10.1038/nature01898

Wang, R. C., Smogorzewska, A., & de Lange, T. (2004). Homologous Recombination Generates T-Loop-Sized Deletions at Human Telomeres. *Cell*, *119*(3), 355-368. https://doi.org/https://doi.org/10.1016/j.cell.2004.10.011

Wang, X., Le, N., Denoth-Lippuner, A., Barral, Y., & Kroschewski, R. (2016). Asymmetric partitioning of transfected DNA during mammalian cell division. *Proceedings of the National Academy of Sciences of the United States of America*, *113*(26), 7177-7182. https://doi.org/https://doi.org/10.1073/pnas.1606091113

Warecki, B., Ling, X., Bast, I., & Sullivan, W. (2020). ESCRT-III–mediated membrane fusion drives chromosome fragments through nuclear envelope channels. *The Journal of Cell Biology*, *219*(3), e201905091. https://doi.org/10.1083/jcb.201905091 PMID - 32032426

Ye, Q., & Worman, H. J. (1996). Interaction between an Integral Protein of the Nuclear Envelope Inner Membrane and Human Chromodomain Proteins Homologous to Drosophila HP1*. *Journal of Biological Chemistry*, *271*(25), 14653-14656. https://doi.org/10.1074/jbc.271.25.14653 PMID - 8663349

Zhang, C.-Z., Spektor, A., Cornils, H., Francis, J. M., Jackson, E. K., Liu, S., Meyerson, M., & Pellman, D. (2015). Chromothripsis from DNA damage in micronuclei. *Nature*, *522*(7555), 179 - 184. https://doi.org/10.1038/nature14493

Zheng, R., Ghirlando, R., Lee, M. S., Mizuuchi, K., Krause, M., & Craigie, R. (2000). Barrier-to-autointegration factor (BAF) bridges DNA in a discrete, higher-order nucleoprotein complex. *Proceedings of the National Academy of Sciences of the United States of America*, *97*(16), 8997 - 9002. https://doi.org/10.1073/pnas.150240197

Fig. 1

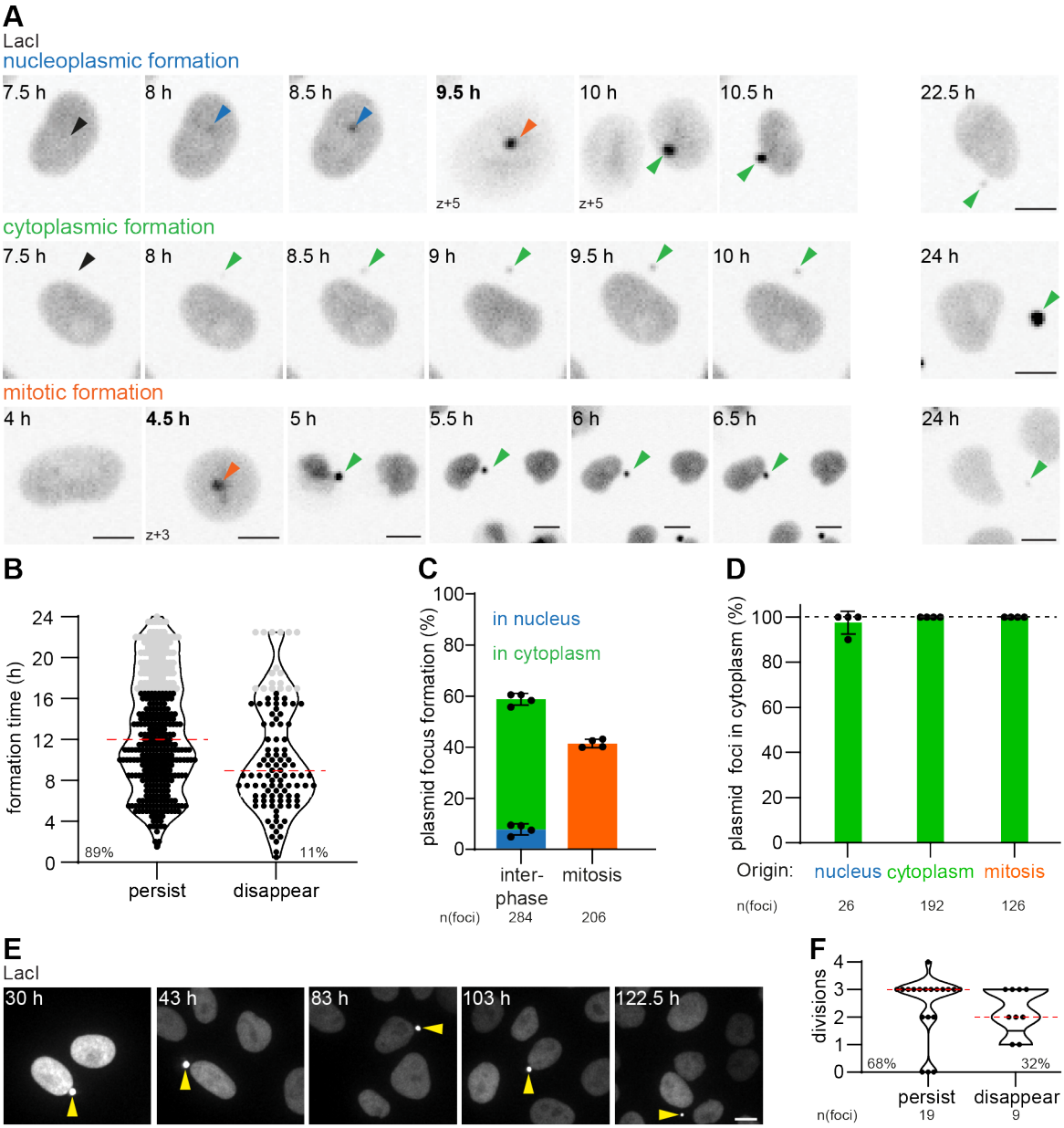

Cytoplasmic plasmid foci have 3 origins and are maintained in the cytoplasm long-term.

(**A**) Time-lapse images of plasmid focus formations in HeLa-LacI cells transfected at imaging start with pLacO. Scale bar, 10 µm. Time, after lipofection; bold time, mitosis. Arrowheads: nucleoplasmic focus, blue; cytoplasmic, green; mitosis, orange; future focus formation, black. Single z-slices. (**B**) Timing of individual focus formation events (circle) after pLacO lipofection. Persisting (persist) and disappearing (disappear) foci. 4 experiments (exp.) pooled; n(foci): 490; median, red. Last 25 % of all appearances, grey. % relative to all foci formed. (**C**) Focus formations in interphase or mitotic cells relative to all plasmid focus formations. 1 exp., circle; mean & SD. (**D**) Foci that are in the cytoplasm at imaging end depending on their origin. Last 25 % formations (in B) excluded. Color code as in (A). n(foci): 344; 100 % reference, dashed line. (**E,F**) Imaging started 30 hours after pLacO lipofection. 1 exp., n(cells): 28. (**E**) Time-lapse images of a pLacO transfected cell with one persisting focus, yellow arrowhead. Images, maximum intensity (max.) projected; (**F**) Maximal number of divisions a plasmid focus was detectable. One focus, circle. Persisting (persist) until imaging end or disappearing before (disappear); % relative to all foci.

Fig. 2

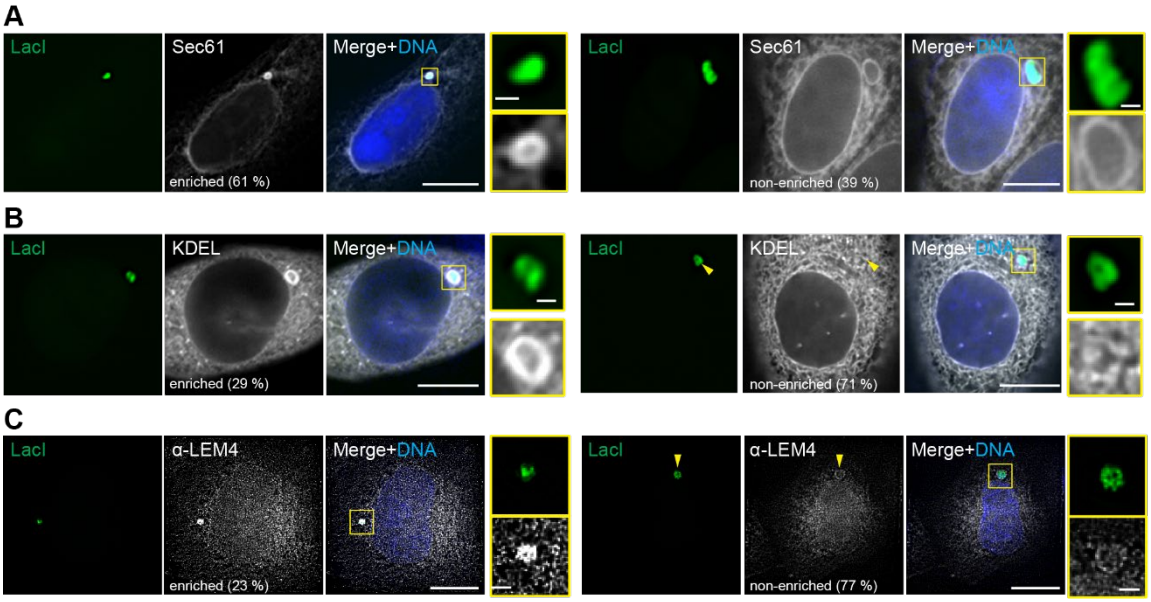

ER enwraps cytoplasmic plasmid DNA.

(**A-C**) Representative images of the localization of ER reporters in pLacO transfected HeLa-LacI cells 24 hours after lipofection with the frequency of two localization patterns (enriched and non-enriched, relative to the intensity of the surrounding ER). DNA, blue (Hoechst stain). Single z-slice images deconvolved. Insets: plasmid focus; scale bars: in big images: 10 µm, in insets: 1 µm. (**A**) Transient expression of Sec61-mCherry. Pooled data of 4 exp., total n(cells): 76. n(foci): 79. % relative to all foci analyzed. (**B**) Transient expression of GFP-KDEL. Arrowhead, position of plasmid focus; 3 exp.; total n(cells): 80; n(foci): 96. % relative to all foci analyzed. (**C**) Anti-LEM4 immunostaining 24 hours after pLacO lipofection. 2 exp. n(cells): 84; n(foci): 84. % relative to all foci analyzed.

Fig. 3

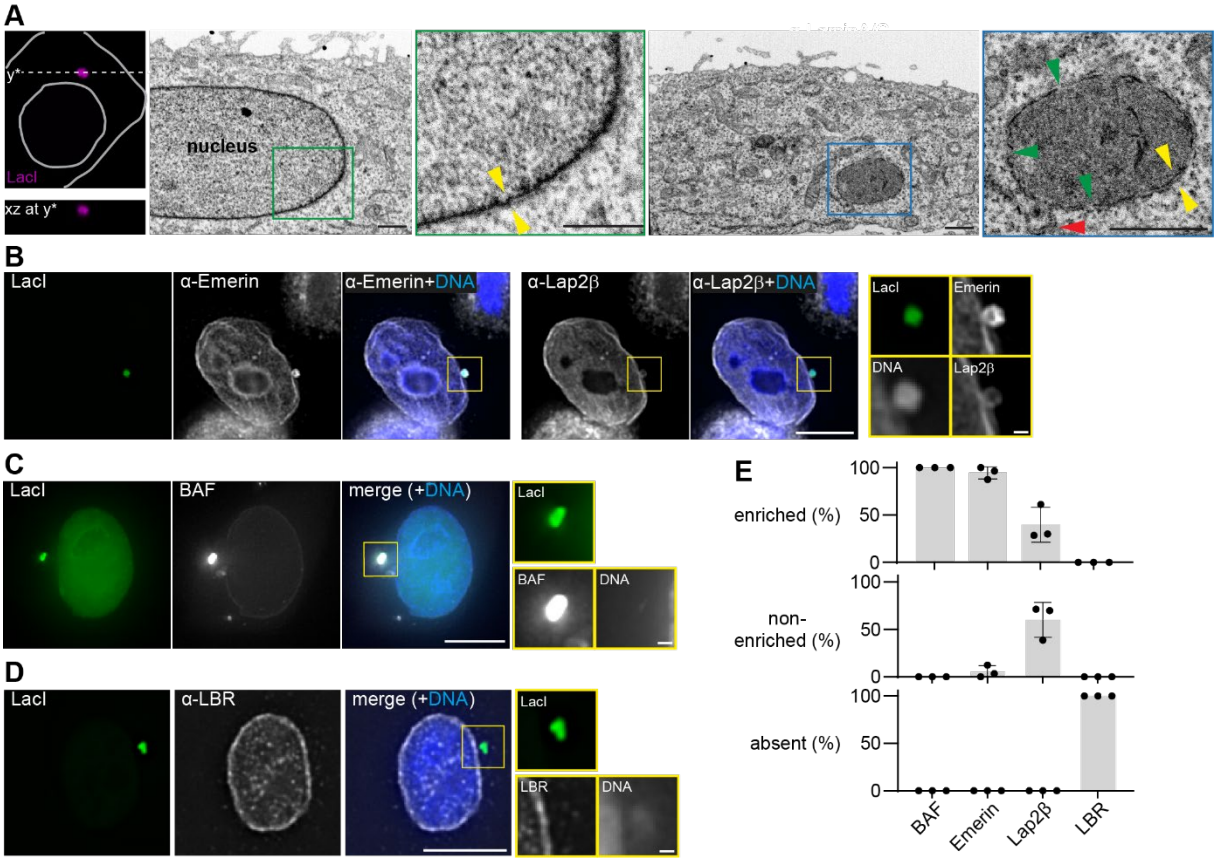

A special double membrane enwraps cytoplasmic plasmid DNA.

(**A**) Correlative fluorescence with electron microscopy (CLEM) of an interphase cell containing one pLacO focus. Left images: confocal images; upper: single z-slice xy-image superimposed with a grey cell outline and the y*-cut line; lower: xz-view of the upper cell along the dashed y* line. The first overview EM image depicts a part of the nucleus of the cell shown in the confocal images. The second overview EM image corresponds to the same cell imaged at y*. Insets: plasmid focus, blue square; part of the interphase nucleus, green square; double-layered NE, yellow arrowhead pair; membrane connecting proximal ER and the plasmid focus, red arrowhead; gaps in the focus envelope, green arrowheads; scale bars 1 µm. (**B-D**) Representative images of the localization of indicated reporters and plasmid foci in HeLa-LacI. Images: single z-slice, deconvolved; insets: plasmid foci; scale bars: in big images 10 µm; in insets: 1 µm; DNA, blue (Hoechst stain). (**E**) Quantification of relative localization patterns (absent, non-enriched, enriched relative to the NE) of indicated reporters 24 hours after lipofection of pLacO. 3 exp. (circles); mean and SD, each with total numbers: n(Lap2β, foci): 52; n(Emerin, foci): 62; n(LBR, foci): 63; n(LBR, cells): 54; n(BAF, foci): 23; n(BAF, cells): 23.

Fig. 4

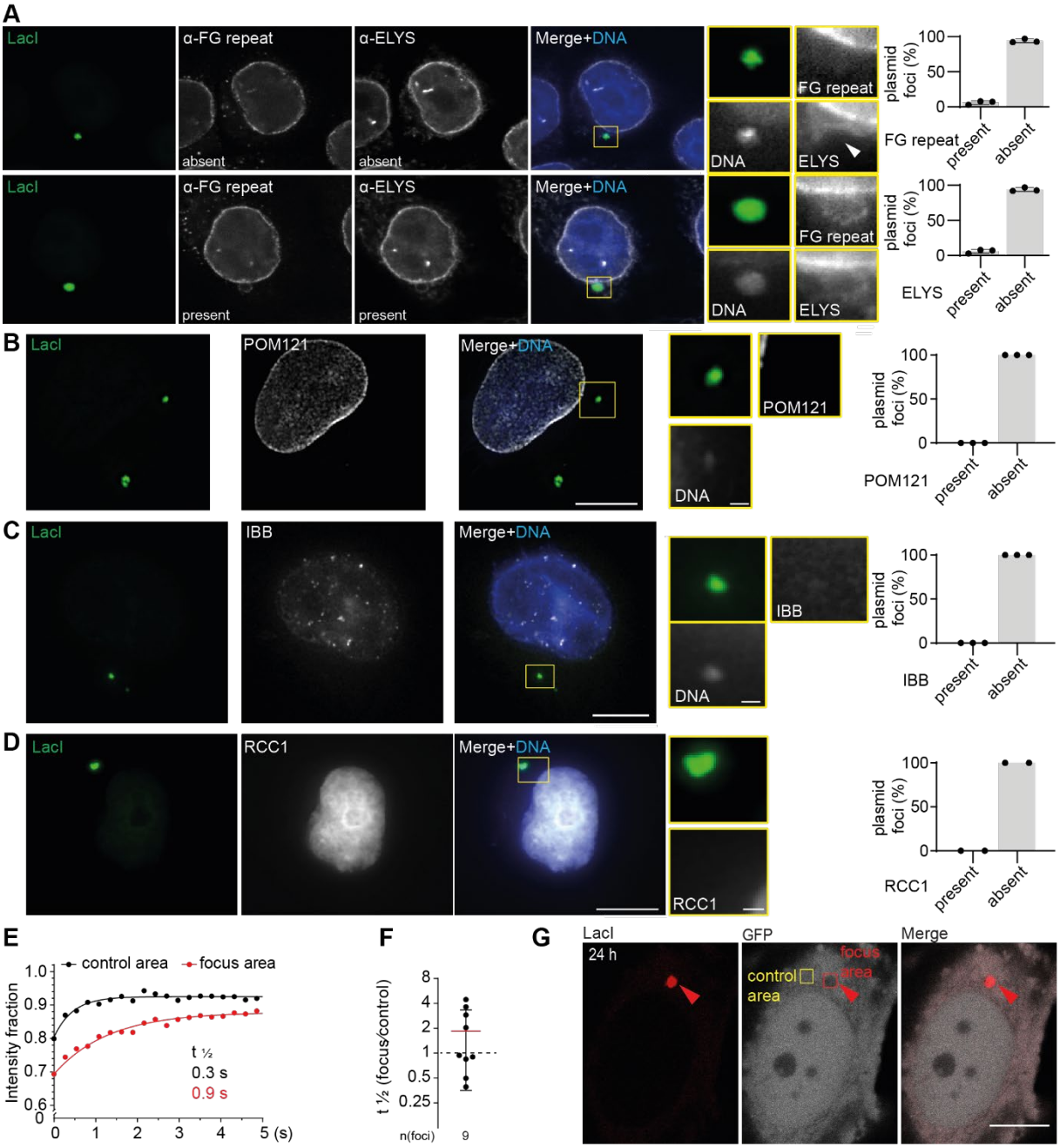

The plasmid enwrapping envelope is devoid of functional NPCs but not closed.

(**A-D**) Representative images of HeLa-LacI cells 24 hours after lipofection with pLacO. Insets: plasmid focus; scale bars: in big images: 10 µm, in insets: 1 µm; focus, arrowheads. DNA, blue (Hoechst stain). Right quantification; % relative to all foci; 1 exp., circle. (**A**) Immunostaining for ELYS and FG-repeats. Upper: absence, lower: presence example, 3 exp.; mean & SD; n(ELYS, FG-repeats, foci): 111. (**B-D**) Images (single z-slice, deconvolved) and quantification. (**B**) POM121. 3 exp.; n(foci): 55. (**C**) IBB. 3 exp.; n(foci): 22; n(cells): 17. (**D**) RCC1. 2exp.; n(foci): 55; n(RCC1, cells): 48. (**E-G**) FRAP analysis in HeLa cells transiently expressing LacI-mCherry and soluble GFP 24 hours after pLacO transfection. (**E**) Recovery of bleached GFP over time; $t_{1/2:}$ recovery time for half of GFP intensity. (**F**) Quantification of (E): Ratio of $t_{1/2}$ at focus area versus control area. Mean & SD; 3 exp.; n(foci): 9. (**G**) Representative images of bleaching areas. Focus area, red square; control area, yellow area. Scale bar: 10 µm.

Fig. 5

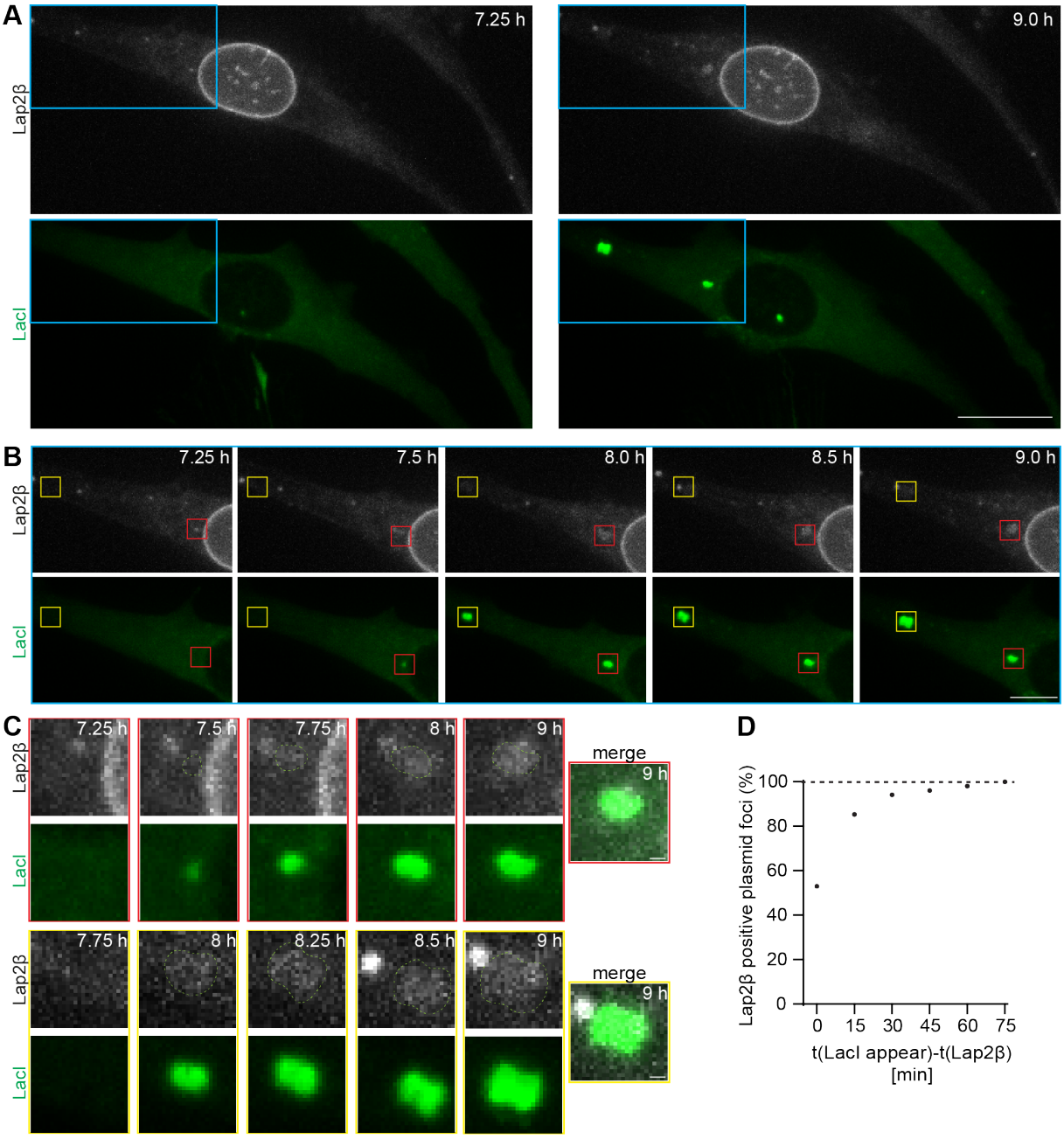

A plasmid focus formed in the cytoplasm is rapidly enwrapped by membrane.

(**A-C**) Time-lapse images of HeLa cells stably expressing Lap2β-GFP (Lap2β) and transiently expressing LacI-mCherry (LacI) after lipofection with pLacO. Time, hours after pLacO transfection. (**A**) Overview images of the cell at 7.25 hours and 9 hours after transfection. The area in the blue square is enlarged in B). Scale bar, 20 µm. (**B**) Enlarged part of the cell in (A). Plasmid focus forms with concomitant Lap2β association, red square. Plasmid focus forms with no observable Lap2β association during imaging, yellow square; scale bar, 10 µm. (**C**) Enlarged squares of (B). Both examples show Lap2β association 15 min after LacI fluorescence appearance; outline the focus, superimposed dashed line; lower row: Lap2β channel boosted, non-boosted images in A,B; scale bar, 1 µm. (**D**) Cumulative fraction of plasmid foci associated with Lap2β in dependence on the duration of Lap2β association after focus appearance. 1 exp., total n(foci): 105; n(cells): 49.

Fig. 6

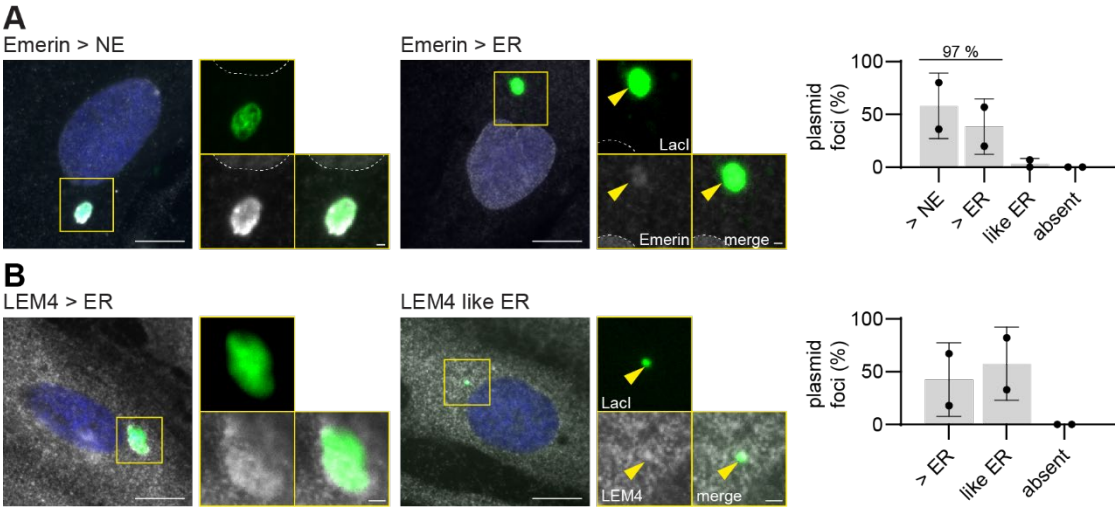

Exclusomes containing plasmid DNA exist in primary human fibroblasts.

(**A+B**) Primary human fibroblasts 48 hours after lipofection with pLacO and plasmid encoding LacI-NLS-GFP immunostained for Emerin (A) and LEM4 (B). Single z-slice images. Insets: plasmid focus; scale bars: in big images 10 µm; in insets: 1 µm; DNA, blue (Hoechst stain). (**A**) Representative images of indicated classification. Outline of nucleus, dashed line. Right graph: Emerin's intensity relative to the NE (> NE) and the ER (> ER, like ER) in cells with 1 cytoplasmic focus. 2 exp. (circles), mean and SD; n(foci): 29. (**B**) Representative images for indicated classification of LEM4. Right graph: LEM4 intensity at plasmid focus relative to the ER (> ER, like ER) in cells with 1 cytoplasmic focus. 2 exp. (circles); mean and SD; n(foci): 38.

Fig. 7

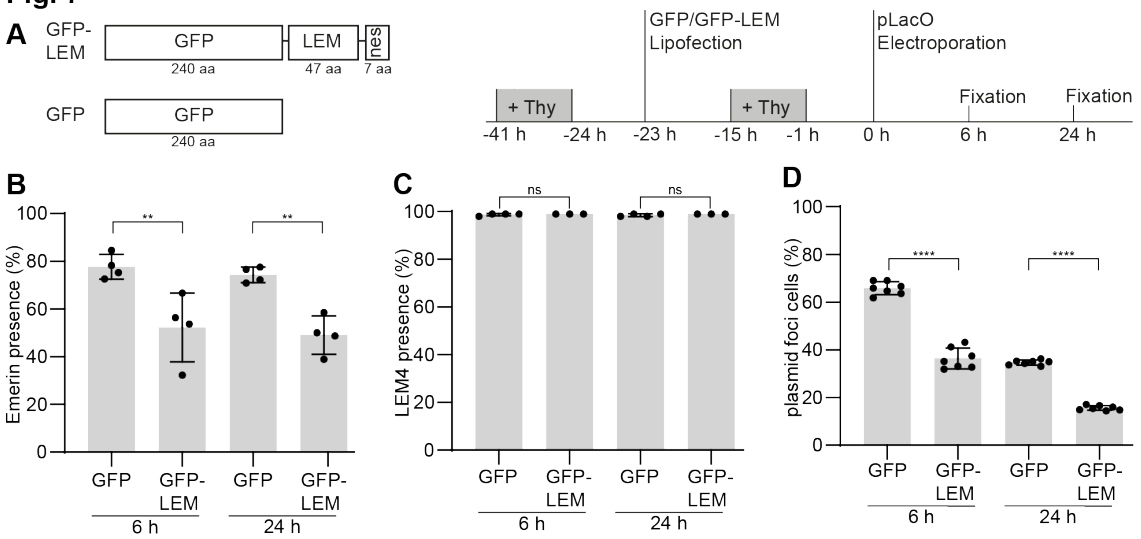

Overexpression of Emerin's LEM domain reduces cells with plasmid foci.

(**A**) Scheme of fusion proteins transiently overexpressed in HeLa-LacI cells (left side) and experimental procedure (right side). GFP-LEM-nes ("GFP-LEM"), soluble GFP ("GFP"); aa: amino acid residues. + Thy: thymidine treatment; time, relative to pLacO transfection. (**B**) Presence of Emerin at cytoplasmic plasmid foci 6 hours and 24 hours after electroporation of pLacO. 4 exp. (circles); mean and SD; two-way Anova, **, $p < 0.01$; n(foci): GFP 6 hours: 589; GFP 24 hours: 458; GFP-LEM 6 hours: 474; GFP-LEM 24 hours: 413. (**C**) Presence of LEM4 at cytoplasmic foci 6 hours and 24 hours after electroporation of pLacO. 3 to 5 exp.(circles); mean and SD; two-way Anova; n.s. not significant; n(foci): GFP 6 hours: 727; GFP 24 hours: 536; GFP-LEM 6 hours: 334; GFP-LEM 24 hours: 280. (**D**) Frequency of cells containing at least one cytoplasmic focus in GFP and GFP-LEM expressing cells 6 hours and 24 hours after electroporation. 7 exp. (circles); mean and SD; two-way Anova; **** $p<0.0001$; n(cells): GFP 6 hours: 1428; GFP 24 hours: 1460; GFP-LEM 6 hours: 1471; GFP-LEM 24 hours: 1469.

Fig. 8

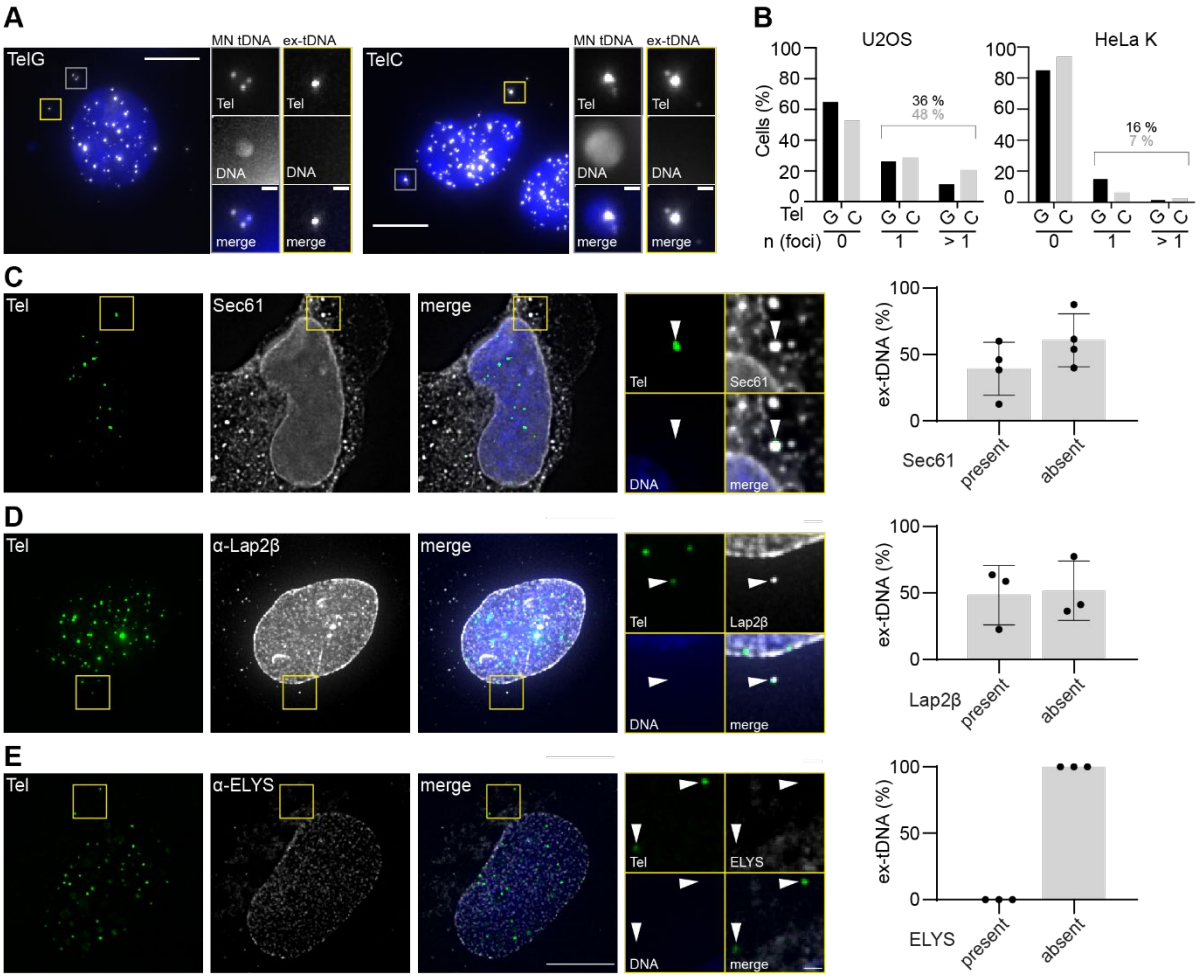

A special envelope enwraps also cytoplasmic extra-chromosomal telomeric DNA.

(**A**) Representative images of U2OS cells FISH stained with TelG and TelC probes. Images max. projected, insets: area with ex-tDNA, yellow squares; area with MN tDNA, gray squares. Scale bars: in big images: 10 µm; in insets: 1 µm. DNA, blue (Hoechst stain). (**B**) Frequency of HeLa K and U2OS cells with none, one (1), or more than one (>1) ex-tDNA focus relative to the total cells analyzed. Pooled data of FISH experiments. U2OS-TelG probe: 3 exp.; >47 cells/exp., total n(cells): 217; U2OS-TelC probe: 3 exp.; >49 cells/exp., total n(cells): 171; HeLa-TelG probe: 3 exp.; >55 cells/exp., total n(cells): 210; HeLa-TelC probe: 3 exp.; > 63 cells/exp., total n(cells): 209. (**C-E**) Representative single z-slice images of FISH-IF stained U2OS cells depicting the localization of the reporter proteins (left); quantification of colocalization of respective marker at ex-tDNA focus (right, plot). Big images: max. projected deconvolved images; arrowheads, ex-tDNA foci ; insets: areas of tDNA foci. Scale bars: big images: 10 µm, insets: 1 µm; 3 exp.; DNA, blue (Hoechst stain). Signals of TelG probe, overexpressed of Sec61-mCherry (C) and indicated antibodies (D,E) are displayed. % relative to all ex-tDNA foci analyzed. Mean & SD. Sec61, 4 exp. (circles), n(Sec61, ex-tDNA): 95; Lap2β, 3 exp. (circles), n(Lap2β, ex-tDNA):1 54; ELYS, 3 exp. (circles), n(ELYS, ex-tDNA): 66.

Fig. 9

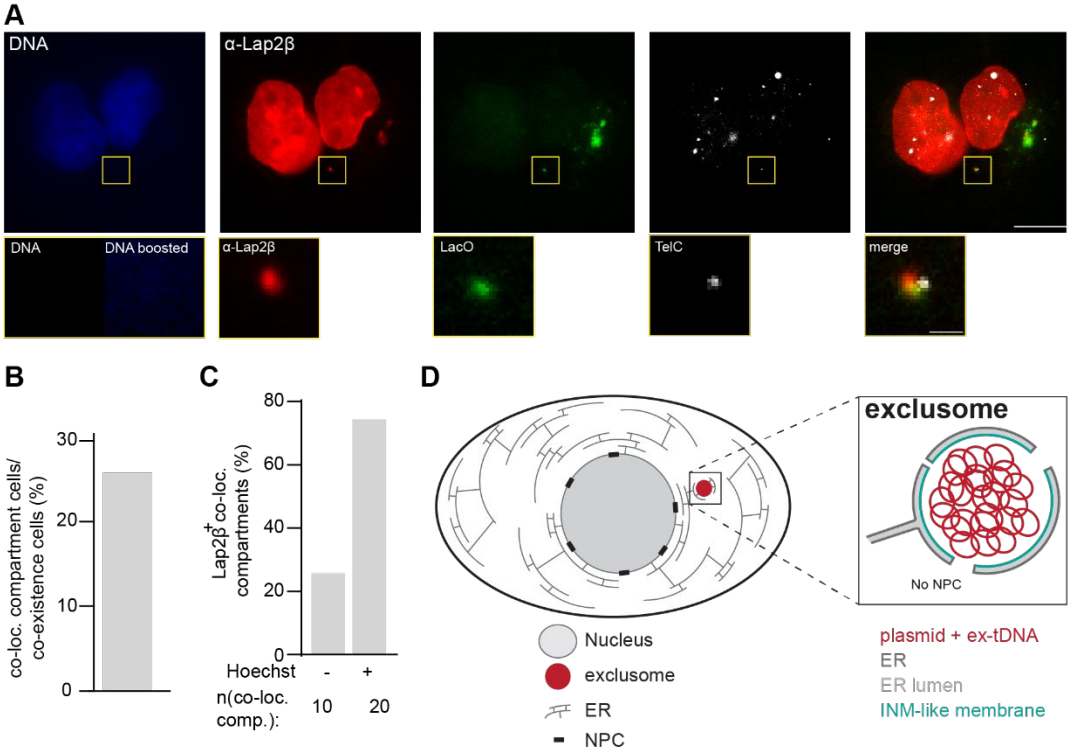

Plasmid DNA and ex-tDNA can be clustered in one exclusome.

(**A**) Representative image of a U2OS cell transfected with pLacO, fixed, hybridized with TelC and LacO probes and immunostained against Lap2β. DNA, blue (Hoechst stain). Inset: cytoplasmic compartment with two DNA species; DNA stain inset boosted, DNA boosted. Scale bars: in big images: 10 µm, in insets: 1 µm. (**B**) Frequency of U2OS cells with minimally one co-localization compartment in cells, which contain both DNA species (co-existence cells) 24 hours after pLacO transfection. Pooled data of 3 exp., individual exp. in SFig. 8G. >15 co-localization compartments/exp.; total n(co-existence cells): 155; >3 co-existence cells/exp; total n(co-existence cells): 40. (**C**) Frequency of Lap2β positive cytoplasmic co-localizing compartments. 24 hours after pLacO transfection. Pooled data of 3 exp.; individual exp. in SFig. 8H. >3 co-localizing compartment/exp., total: n(Lap2β+ co-localizing compartment): 30. (**D**) Model of an exclusome in an interphase cell. Overview of a cell with nucleus, ER and exclusome (inlet: the magnified exclusome with details).